



CERN-PH-EP-2015-161
29 June 2015

ϕ -meson production at forward rapidity in p-Pb collisions at $\sqrt{s_{NN}} = 5.02$ TeV and in pp collisions at $\sqrt{s} = 2.76$ TeV

ALICE Collaboration*

Abstract

The first study of ϕ -meson production in p-Pb collisions at forward and backward rapidity, at a nucleon-nucleon centre-of-mass energy $\sqrt{s_{NN}} = 5.02$ TeV, has been performed with the ALICE apparatus at the LHC. The ϕ -mesons have been identified in the dimuon decay channel in the transverse momentum (p_T) range $1 < p_T < 7$ GeV/ c , both in the p-going ($2.03 < y < 3.53$) and the Pb-going ($-4.46 < y < -2.96$) directions — where y stands for the rapidity in the nucleon-nucleon centre-of-mass — the integrated luminosity amounting to 5.01 ± 0.19 nb $^{-1}$ and 5.81 ± 0.20 nb $^{-1}$, respectively, for the two data samples. Differential cross sections as a function of transverse momentum and rapidity are presented. The forward-backward ratio for ϕ -meson production is measured for $2.96 < |y| < 3.53$, resulting in a ratio ~ 0.5 with no significant p_T dependence within the uncertainties. The p_T dependence of the ϕ -meson nuclear modification factor R_{pPb} exhibits an enhancement up to a factor 1.6 at $p_T = 3-4$ GeV/ c in the Pb-going direction. The p_T dependence of the ϕ -meson cross section in pp collisions at $\sqrt{s} = 2.76$ TeV, which is used to determine a reference for the p-Pb results, is also presented here for $1 < p_T < 5$ GeV/ c and $2.5 < y < 4$, for a 78 ± 3 nb $^{-1}$ integrated luminosity sample.

© 2015 CERN for the benefit of the ALICE Collaboration.

Reproduction of this article or parts of it is allowed as specified in the CC-BY-4.0 license.

*See Appendix A for the list of collaboration members

1 Introduction

Proton-nucleus (p-A) collisions are of special interest in the context of high-energy nuclear physics for two reasons. On one hand, a precise characterisation of particle production processes in p-A collisions is needed as a reference for nucleus-nucleus data. This allows in-medium effects — linked to the formation of a deconfined phase of the QCD matter, the quark-gluon plasma (QGP) [1–3] — to be disentangled from the effects already present in cold nuclear matter. Among them, a sizeable role is played by the transverse momentum broadening of initial-state partons due to multiple scattering inside the nucleus, responsible for the Cronin effect [4], which may lead to an enhancement of intermediate- p_{T} hadron spectra. In addition, p-A collisions at LHC energies provide a way to probe the parton distributions of the colliding nucleus at small values of Bjorken- x , in a regime where parton densities can reach saturation [5, 6]. In particular, the smallest x values contributing to the wave function of the colliding nucleus can be probed by looking at particle production at large rapidities, in the p-going direction. Such a measurement can thus extend towards lower x -values the results of the lower-energy measurements by the PHOBOS and BRAHMS experiments at RHIC [7, 8]. Measurements of identified particle production may, in particular, provide useful constraints for forthcoming theoretical studies of the saturation mechanism at small x .

We have already reported results on charged particle production in p-Pb collisions at mid-rapidity. These results focused on the pseudorapidity density [9] and the p_{T} dependence of the nuclear modification factor [10–12]; the latter was found to be consistent with unity for $p_{\text{T}} \gtrsim 2$ GeV/ c . The nuclear modification factor of charged hadrons was also studied by the BRAHMS and PHOBOS Collaborations in d-Au collisions at the nucleon-nucleon centre-of-mass energy $\sqrt{s_{\text{NN}}} = 200$ GeV at RHIC [13, 14], as a function of pseudorapidity, where values smaller than unity were found for $\eta \gtrsim 1$, corresponding to the d-going direction.

In this Letter we report the measurement of ϕ -meson production at forward rapidity in p-Pb collisions at $\sqrt{s_{\text{NN}}} = 5.02$ TeV in the transverse momentum (p_{T}) range $1 < p_{\text{T}} < 7$ GeV/ c , for the centre-of-mass rapidity (y) ranges $2.03 < y < 3.53$ (p-going direction) and $-4.46 < y < -2.96$ (Pb-going direction), in the dimuon decay channel with the ALICE detector. This measurement extends the investigation of light-flavour particle production to forward rapidity. At the same time, it represents an essential baseline for the understanding of ϕ production in heavy-ion collisions, where an enhancement of strange particle yields relative to the ones measured in pp collisions has been proposed long ago as a signature of the formation of a QGP phase [15–17] triggering an intense experimental effort already at SPS and RHIC energies [18–24]. It should be noted that, despite its hidden strangeness, producing a ϕ -meson in a hadronic collision still implies the creation of a $s\bar{s}$ pair as it is the case for other strange hadrons, even if the hadronisation mechanisms can differ in reason of the different quark composition. In this context, the p-Pb data presented here will provide an important reference for future measurements in Pb-Pb collisions in the LHC Run 2, which will be performed at a comparable energy.

The differential ϕ -meson cross section as a function of transverse momentum is also presented for pp collisions at $\sqrt{s} = 2.76$ TeV. This measurement complements the ALICE results on ϕ -meson production in pp collisions at $\sqrt{s} = 7$ TeV, already reported in [25] and, combined with the latter, is used to build the pp reference for the p-Pb measurements presented here.

2 Experimental setup

A full description of the ALICE detector can be found in [26, 27]. The results presented in this Letter have been obtained detecting muon pairs with the muon spectrometer, covering the pseudorapidity region $-4 < \eta_{\text{lab}} < -2.5$. Here and in the following, the sign of η_{lab} is determined by the choice of the LHC reference system. The other detectors relevant for the analysis are the Silicon Pixel Detector (SPD) of the Inner Tracking System (ITS), the V0 detector and the Zero Degree Calorimeters (ZDC).

The elements of the muon spectrometer are a hadron absorber, followed by a set of tracking stations, a dipole magnet, an iron wall acting as muon filter and a set of trigger stations. The hadron absorber is made of carbon, concrete and steel and is placed 0.9 m away from the interaction point. Its total material budget corresponds to 10 hadronic interaction lengths. The dipole magnet provides an integrated magnetic field of $3 \text{ T} \cdot \text{m}$ in the vertical direction. The muon tracking is provided by five tracking stations, each one composed of two cathode pad chambers. The first two stations are located upstream of the dipole magnet, the third one in the middle of its gap and the last two downstream of it. A 1.2 m thick iron wall, corresponding to 7.2 hadronic interaction lengths, is placed between the tracking and trigger detectors and absorbs the residual secondary hadrons emerging from the hadron absorber. The hadron absorber together with the iron wall stops muons with total momentum lower than $\sim 4 \text{ GeV}/c$. The muon trigger detector consists of two stations, each one composed of two planes of resistive plate chambers, installed downstream of the muon filter.

The SPD consists of two silicon pixel layers, covering the pseudorapidity regions $|\eta_{\text{lab}}| < 2.0$ and $|\eta_{\text{lab}}| < 1.4$ for the inner and outer layer, respectively. It is used for the determination of the primary interaction vertex position. The V0 is composed of two scintillator hodoscopes covering the pseudorapidity regions $2.8 < \eta_{\text{lab}} < 5.1$ and $-3.7 < \eta_{\text{lab}} < -1.7$. It is used in the definition of the minimum bias trigger signal, and allows the offline rejection of beam-halo and beam-gas interactions to be performed. The ZDC detectors, positioned symmetrically at 112.5 m from the interaction point, are used to clean the event sample by removing beam-beam collisions not originating from nominal LHC bunches.

3 Data selection and signal extraction

The analysis presented in this Letter is based on two data samples, collected by ALICE during the 2013 p-Pb and pp runs at $\sqrt{s_{NN}} = 5.02$ TeV and $\sqrt{s} = 2.76$ TeV, respectively. In this section we present the details of the data selection, as well as the procedure followed for the extraction of the ϕ -meson signal.

3.1 Data selection

The Minimum-Bias (MB) trigger for the considered data sample is given by the logical AND of the signals in the two V0 detectors [28]. Events containing a muon pair are selected by means of a specific dimuon trigger, based on the detection of two muon candidate tracks in the trigger system of the muon spectrometer, in coincidence with the MB condition. Due to the intrinsic momentum cut imposed by the detector, only muons with $p_T \gtrsim 0.5 \text{ GeV}/c$ manage to leave a signal in the trigger chambers.

Because of the different energy of the LHC proton and Pb beams ($E_p = 4 \text{ TeV}$, $E_{\text{Pb}} = 1.58 \text{ A} \cdot \text{TeV}$), in p-Pb collisions the nucleon-nucleon centre-of-mass moves in the laboratory with a rapidity $y_0 = 0.465$ in the direction of the proton beam. The directions of the proton and Pb beam orbits were inverted during the p-Pb data taking period. This allowed the ALICE muon spectrometer to access two different rapidity regions¹: the region $2.03 < y < 3.53$ where the proton beam is directed towards the muon spectrometer (p-going direction) and the region $-4.46 < y < -2.96$ where the Pb beam is directed towards the muon spectrometer (Pb-going direction). In the following, these two rapidity ranges are also referred to as “forward” and “backward”, respectively. For pp collisions at $\sqrt{s} = 2.76 \text{ TeV}$ the muon spectrometer covers the rapidity region $2.5 < y < 4$ ².

Background events not coming from beam-beam interactions are rejected by performing an offline selection, based on the requirement that the timing signals from the V0 and ZDC detectors are compatible with a collision occurring in the fiducial interaction region $|z_{\text{vtx}}| \lesssim 10 \text{ cm}$.

The integrated luminosity for the p-Pb data samples was evaluated as $L_{\text{int}} = N_{\text{MB}}/\sigma_{\text{MB}}$, where N_{MB} is

¹ The sign of y is defined by assuming the proton beam to have positive rapidity.

² In this case the sign of y is defined by assuming the proton beam entering the muon spectrometer to have positive rapidity.

the number of MB events corresponding to the analysed triggered events, and σ_{MB} the MB trigger cross section. The value of N_{MB} was obtained by averaging the results of two different methods — one based on the ratio of trigger rates and the other based on the offline selection of dimuon events in the MB data sample [29] — while the MB trigger cross sections σ_{MB} were measured with a van der Meer scan and found to be 2.09 ± 0.07 b and 2.12 ± 0.07 b, respectively, for the beam configurations corresponding to the forward and backward rapidity coverage of the muon spectrometer [30]. For the pp data sample, the integrated luminosity is calculated with the method described in [31], using as reference the MB trigger cross section $\sigma_{\text{MB}} = 47.7 \pm 0.9$ mb, measured in a van der Meer scan [32].

The resulting values of L_{int} for the analysed p-Pb data samples are 5.01 ± 0.19 nb $^{-1}$ and 5.81 ± 0.20 nb $^{-1}$ [29, 30] — corresponding to ~ 24000 and ~ 26000 reconstructed $\phi \rightarrow \mu\mu$ decays (see next section) — respectively for the forward and backward rapidity regions. For the pp data sample, the integrated luminosity amounts to 78 ± 3 nb $^{-1}$ for a total number of ~ 1400 reconstructed $\phi \rightarrow \mu\mu$ decays.

Track reconstruction in the muon spectrometer is based on a Kalman filter algorithm [25, 33, 34]. Muon identification is performed by requiring the candidate track to match a track segment in the trigger chambers (trigger tracklet). This request selects muons with $p_{\text{T},\mu} \gtrsim 0.5$ GeV/ c and, as a consequence, significantly affects the collected statistics for dimuons with invariant mass $\lesssim 1$ GeV/ c^2 and $p_{\text{T}} \lesssim 1$ GeV/ c . It is also required that muon tracks lie in the pseudorapidity interval $-4 < \eta_{\mu} < -2.5$, where η_{μ} is defined in the laboratory frame, in order to remove the tracks close to the acceptance borders of the spectrometer, where the acceptance drops abruptly. Selected tracks are finally required to exit the hadron absorber at a radial distance from the beam axis, R_{abs} , in the range $17.6 < R_{\text{abs}} < 89.5$ cm: this cut, for all practical purposes equivalent to the one on η_{μ} , explicitly ensures the rejection of tracks crossing the region of the absorber with the highest density material, where multiple scattering and energy loss effects are large and can affect the mass resolution. Muon pairs are built combining two muon tracks that satisfy the above cuts.

3.2 Signal extraction

The Opposite-Sign (OS) muon pairs are composed of correlated and uncorrelated pairs. The former contain the signal of interest for the present analysis, while the latter — mainly coming from semi-muonic decays of pions and kaons — form a combinatorial background. The contribution of the combinatorial background to the OS mass spectrum was evaluated using an event mixing technique in which uncorrelated pairs are formed with muons taken from different events. A detailed description of the technique can be found in [25]. The ratio between correlated and uncorrelated OS dimuons at the ϕ -meson mass is ~ 0.65 (~ 0.40) in p-Pb collisions at $\sqrt{s_{\text{NN}}} = 5.02$ TeV at forward (backward) rapidity, and ~ 1.30 in pp collisions at $\sqrt{s} = 2.76$ TeV. A direct comparison of the raw OS mass spectrum and the associated combinatorial background is presented in [35], for each of the p_{T} intervals considered in the analysis.

The invariant mass spectra in pp and p-Pb collisions, obtained after combinatorial background subtraction, are shown in Fig. 1 for the p_{T} -integrated samples. In the left-column panels of Fig. 1, the signal is described in the low-mass region (from the threshold up to ~ 1.5 GeV/ c^2) by the superposition of a so-called hadronic cocktail and the open charm and open beauty processes. The processes included in the hadronic cocktail are the two-body and Dalitz decays of the light neutral mesons $\eta, \rho, \omega, \eta'$ and ϕ , which dominate dimuon production for invariant masses below ~ 1 GeV/ c^2 . The open charm and open beauty contributions arise from correlated semi-muonic decays of charm and beauty mesons and baryons.

The hadronic cocktail was simulated with a dedicated generator described in [25], tuned to the existing measurements whenever possible, otherwise based on the kinematic distributions extracted from PYTHIA [36]. In particular, the kinematic distributions of the ϕ -meson have been tuned by means of an iterative procedure to the results presented in this Letter to ensure self-consistency for this analysis. The open charm and beauty generation is based on a parameterisation of the spectra generated with PYTHIA [33]. The detector response for all these processes is obtained with a simulation based on the

GEANT3 [37] transport code. Simulated events are then subjected to the same reconstruction and selection procedure as the data.

When describing the signal with the superposition of the aforementioned contributions, four parameters are adjusted in the fit procedure in each of the p_T or rapidity intervals considered in the analysis: the yield of the η , ω and ϕ -mesons, and the one of the open charm and beauty processes, with the relative beauty/charm contribution fixed (see later in this paragraph). In this way, each parameter is linked to a process dominating in at least one region of the considered mass spectrum. The remaining degrees of freedom are fixed either according to the relative branching ratios known from literature [38], or assuming specific hypotheses on the cross section ratios. In particular, the production cross section of the ρ -meson is assumed to be the same as for the ω as suggested from both models and pp data [25], while the η' contribution was derived from the η cross section by applying the ratio of the corresponding cross sections $\sigma_{\eta'}/\sigma_{\eta} = 0.3$ taken from the PYTHIA tunes ATLAS-CSC and D6T which best describe the available low-mass dimuon measurements at the LHC energies [25]. The open beauty normalisation is fixed to the open charm one via a fit of the p_T - and rapidity-integrated mass spectra in which the yields from both processes are free parameters; when performing differential studies, the beauty/charm ratio is scaled according to the differential distributions for the two processes, given by the Monte Carlo (MC) simulations.

For each p_T and rapidity interval, the raw number of ϕ -mesons is determined via a fit procedure based on a χ^2 minimisation, performed on the signal obtained after the subtraction of the combinatorial background, shown in Fig. 1 for the p_T -integrated samples. Several tests have been performed to evaluate the robustness of the signal extraction and estimate an appropriate systematic uncertainty for it. They include in particular:

- Replacing the fit based on the full MC hadronic cocktail with a fit based on the superposition of various empirical functions. In this case, illustrated in the right-column panels of Fig. 1, the continuum is modelled either with exponential functions or variable-width Gaussians, while the $\rho+\omega$ and ϕ -meson peaks are described by Crystal Ball functions [39] tuned on the MC.
- Varying the ratio between the yields of open beauty and open charm processes. It was verified that for perturbations as large as $\pm 50\%$ (resulting in a reasonably wide range of variation for the shape of the total continuum) no significant systematic effect is visible.
- Varying the ratios between the two-body and Dalitz branching ratios of the η and ω -mesons, as well as the cross section ratios $\sigma_{\rho}/\sigma_{\omega}$ and $\sigma_{\eta'}/\sigma_{\eta}$, within the uncertainties coming either from the available measurements or from the differences between the PYTHIA tunes considered in the analysis of the pp data. The branching ratio $BR_{\omega \rightarrow \mu\mu}$ was taken as the average (weighted by the corresponding uncertainties) of the available measurements of $BR_{\omega \rightarrow \mu\mu}$ and $BR_{\omega \rightarrow ee}$ [38], assuming lepton universality.
- Varying the considered fit range: in particular, the fit was performed both including and excluding the mass region from 0.4 to 0.65 GeV/ c^2 where the quality of the comparison between the data and the sum of the MC sources turns out to be lower.

The total systematic uncertainty on the signal extraction was taken as the quadratic sum of the above sources. The systematic uncertainty on the combinatorial background is estimated by comparing the shape of the Like-Sign dimuon contributions coming from the event mixing procedure and from the raw data [25]. This uncertainty depends on the mass, its relative contribution being maximal in the mass window 0.5-0.8 GeV/ c^2 and minimal around the ϕ -meson peak, and it is added in quadrature, for each point of the mass spectrum, to the statistical uncertainty of the signal: in this way, this source of systematics is accounted for by the χ^2 minimisation procedure, and automatically propagated when

evaluating the ϕ -meson raw signal from the fit parameters. The uncertainty associated to the sum of the MC sources (red band in the left-column plots of Fig. 1) is evaluated by combining the uncertainties on the normalisation of each considered process. For the processes whose normalisation is left free in the fit, this uncertainty is the statistical one resulting from the fit procedure itself; for the rest of the processes, we also propagate the systematic uncertainty on the parameters (branching ratios or cross section ratios) which fix their normalisations to those of the free processes.

4 Results

The results of the ϕ -meson analysis are presented as follows. We first present the measurement of the production cross sections, starting with its p_{T} -dependence in pp collisions at $\sqrt{s} = 2.76$ TeV, followed by p-Pb collision results as a function of p_{T} and rapidity. Then, we show the ratio of the cross sections measured in the forward and backward regions, obtained in the common rapidity interval $2.96 < |y| < 3.53$. Finally, the measurement of the nuclear modification factor R_{pPb} as a function of p_{T} is presented, separately for the p-going and the Pb-going directions.

4.1 Production cross section in pp and p-Pb collisions

The cross section σ_{ϕ} was evaluated for each p_{T} and rapidity interval as:

$$\sigma_{\phi}(x) = \frac{N_{\phi \rightarrow \mu\mu}^{\text{raw}}(x)}{[A \cdot \varepsilon](x) \cdot BR_{\phi \rightarrow \mu\mu} \cdot L_{\text{int}}},$$

where x stands for any specific p_{T} or rapidity interval considered. The total systematic uncertainty on $N_{\phi \rightarrow \mu\mu}^{\text{raw}}(x)$, after combining the different sources described above, ranges between 3 % and 8 % depending on the collision system and kinematic range. The branching ratio $BR_{\phi \rightarrow \mu\mu}$ was taken from [38] as the average (weighted by the corresponding uncertainties) of the available measurements of $BR_{\phi \rightarrow \mu\mu}$ and $BR_{\phi \rightarrow ee}$, assuming lepton universality, resulting in a final uncertainty of approximately 1 %. The product of the geometrical acceptance A and the reconstruction efficiency ε has been evaluated by means of MC simulations, using the cocktail predictions for the differential input spectra. The values are obtained as the ratio between the number of dimuons at the output of the reconstruction chain — including the effect of the event selection criteria imposed on the data — and the number of dimuons injected as input.

The uncertainty on $[A \cdot \varepsilon]$ mainly originates from the systematic uncertainty on the dimuon tracking and trigger efficiencies. The systematic uncertainty on the tracking efficiency, amounting to 6 % and 4 % for the backward and forward rapidity regions, respectively, comes from the residual differences between the results of the efficiency-determination method based on reconstructed tracks [29, 40], applied to both data and MC. For the systematic uncertainty on the trigger efficiency, we also refer to the procedure discussed in [29], resulting in an uncertainty of 3.2 % and 2.8 %, respectively, for the backward and forward rapidity regions considered in the analysis. In order to test possible additional systematic effects related to the hardware trigger p_{T} cut, imposing a non-sharp threshold around 0.5 GeV/ c , the analysis was repeated with the additional offline sharp cuts $p_{\text{T},\mu} > 0.5$ GeV/ c and $p_{\text{T},\mu} > 1$ GeV/ c on single muons. For each of the two alternative scenarios, the corresponding measurement of the ϕ -meson cross section was compared to the one coming from the reference analysis: the difference between the results was found to be smaller than the quadratic difference of the statistical uncertainties, showing that no significant bias related to the trigger threshold affects the results [41].

The reported values correspond to a zero-polarisation scenario for the 2-body decay of the ϕ -meson, in the absence of evidence supporting less trivial assumptions (in particular, no measurement of ϕ -meson polarisation is currently available at the LHC energies).

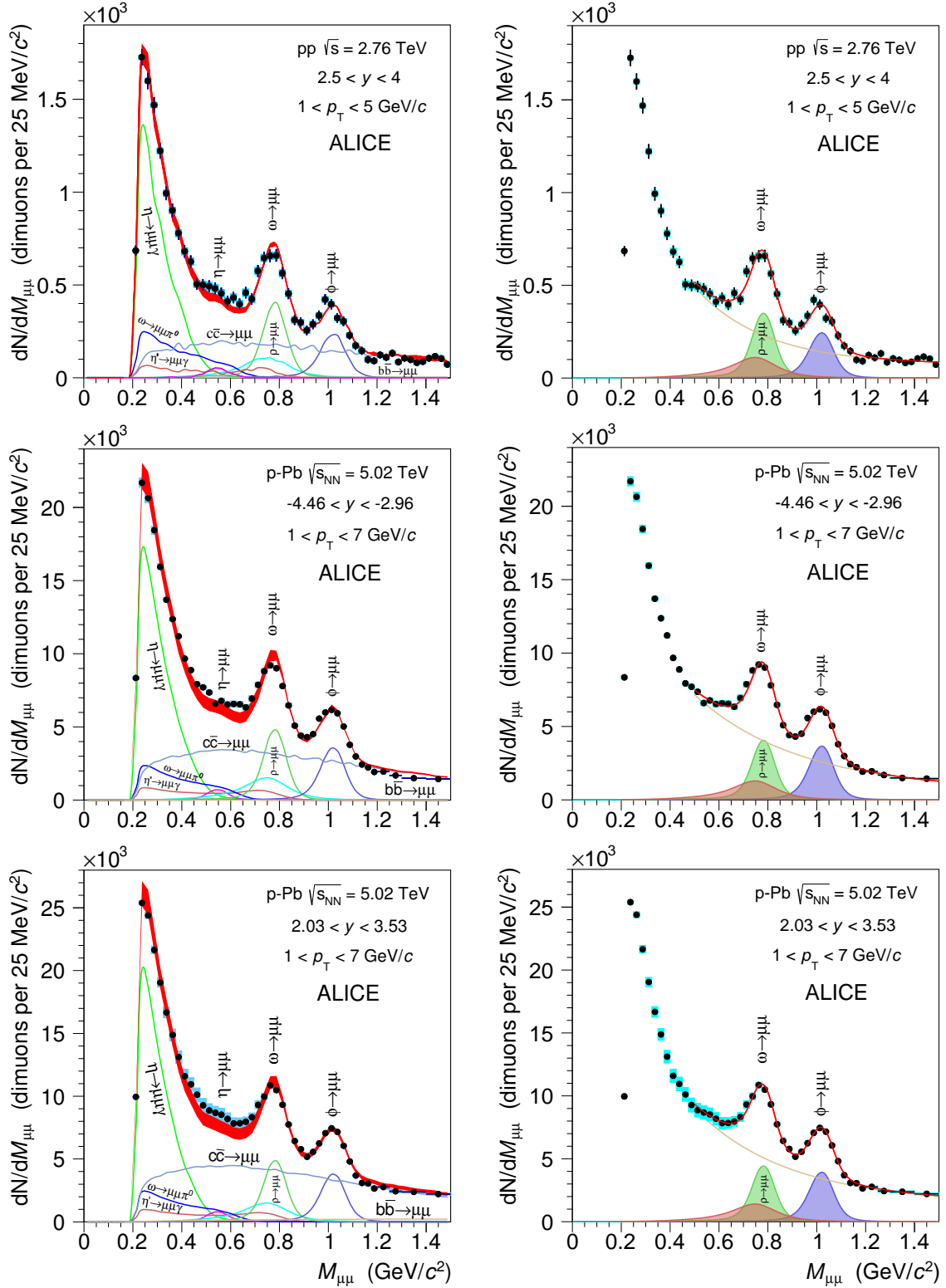


Fig. 1: Dimuon mass spectrum after combinatorial background subtraction: p_T -integrated pp sample (top panels) and p_T -integrated p-Pb sample in the backward (centre panels) and forward (bottom panels) rapidity regions, compared to the result of the hadronic-cocktail and the empirical-function fits (left- and right-column panels, respectively). Error boxes on data points (well visible only in some regions on the plots) represent the systematic uncertainty due to the combinatorial background subtraction, while error bars account for the statistical uncertainty. The width of the hadronic-cocktail fit result (red band) combines the statistical uncertainties of the free fit parameters with the systematic uncertainties on the fixed parameters (see text).

4.1.1 Production cross section in pp collisions

The inclusive, p_T -differential ϕ -meson cross section in pp collisions at $\sqrt{s} = 2.76$ TeV is shown in Fig. 2. The data points, also summarised in Table 1, are compared with the predictions from PHOJET [42] and PYTHIA [36], where for the latter the Perugia0, Perugia11 [43], ATLAS-CSC [44], and D6T [45] tunes are considered. An overall good agreement is found between predictions and data, with the exception of the Perugia0 and Perugia11 tunes of PYTHIA which underestimate the measured cross section by a factor of two, as already observed for the ϕ -meson measurements at $\sqrt{s} = 7$ TeV [25, 46]. It is worth to note that the D6T tune is not successful in describing the p_T evolution of the K/π ratio at mid-rapidity in pp collisions at $\sqrt{s} = 2.76$ TeV, as measured by the CMS Collaboration [47]: this suggests that hidden strangeness is better reproduced than open strangeness in this specific PYTHIA tune. Data points were fitted with a Levy-Tsallis function [48]

$$\frac{1}{p_T} \frac{dN}{dp_T} \propto \left(1 + \frac{m_T - m_\phi}{nT} \right)^{-n}, \quad (1)$$

where $m_T = \sqrt{p_T^2 + m_\phi^2}$ stands for the transverse mass, obtaining the values $n = 10.2 \pm 4.8$ and $T = 284 \pm 72$ MeV for the fit parameters, where the errors reflect the statistical uncertainties only. The cross section integrated over the accessible p_T range $1 < p_T < 5$ GeV/c is $\sigma_\phi = 0.566 \pm 0.055$ (stat.) ± 0.044 (syst.) mb. The systematic uncertainties for this measurement are summarised in Table 2.

4.1.2 Production cross section in p-Pb collisions

The ϕ -meson cross section as a function of p_T in p-Pb collisions is shown in Fig. 3 for the forward and backward rapidity regions considered in the analysis. The results, also reported in Table 3, are fitted with the Levy-Tsallis distribution defined in Eq. (1), the resulting fit parameters being $\beta = 9.6 \pm 1.3$ and $T = 366 \pm 30$ MeV for the forward rapidity region and $\beta = 11.4 \pm 1.4$ and $T = 384 \pm 24$ MeV for the backward one, where the errors reflect the statistical uncertainties only. The predictions from HIJING (with gluon shadowing) [49] and DPMJET [50] are also shown: these generators provided a good

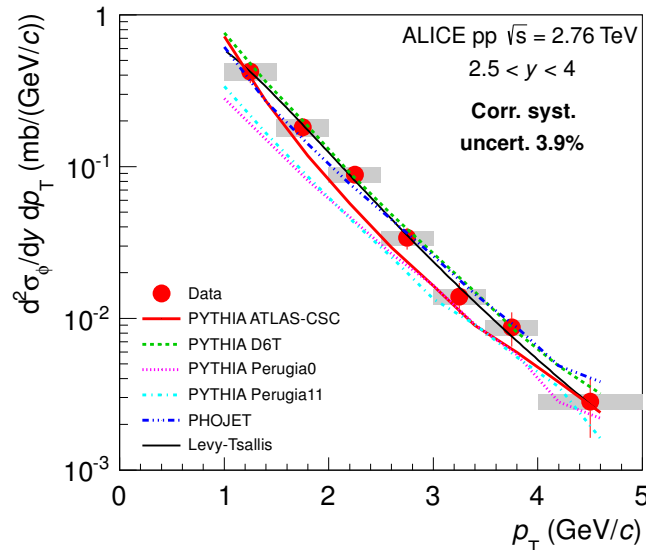


Fig. 2: ϕ -meson cross section as a function of p_T in pp collisions at $\sqrt{s} = 2.76$ TeV. Error bars and boxes represent statistical and systematic uncertainties, respectively. Predictions from PHOJET [42] and the PYTHIA tunes ATLAS-CSC [44], D6T [45], Perugia0 and Perugia11 [43] are also shown for comparison, as well as the result of a fit with the Levy-Tsallis function defined by Eq. (1).

p_T (GeV/c)	χ^2/ndf	$d^2\sigma_\phi/(dydp_T)$ (mb/(GeV/c))
[1.0, 1.5]	1.1	$0.423 \pm 0.067 \pm 0.043$
[1.5, 2.0]	1.7	$0.182 \pm 0.025 \pm 0.018$
[2.0, 2.5]	1.1	$0.089 \pm 0.011 \pm 0.007$
[2.5, 3.0]	1.1	$0.0340 \pm 0.0056 \pm 0.0020$
[3.0, 3.5]	0.9	$0.0139 \pm 0.0032 \pm 0.0011$
[3.5, 4.0]	1.1	$0.0087 \pm 0.0022 \pm 0.0006$
[4.0, 5.0]	1.1	$0.0028 \pm 0.0012 \pm 0.0002$

Table 1: p_T -differential production cross section for the ϕ -meson in pp collisions at $\sqrt{s} = 2.76$ TeV, for $2.5 < y < 4$. The first uncertainty is statistical and the second is the bin-to-bin uncorrelated systematic. The bin-to-bin correlated relative systematic uncertainty is 3.9%. The χ^2/ndf values are relative to the hadronic-cocktail fit and the $[0.8, 1.2 \text{ GeV}/c^2]$ mass region, where $\text{ndf} = 10$.

Source	Syst. uncertainty on σ_ϕ^{pp}
<i>Uncorrelated</i>	
Signal extraction	3–8 %
Tracking efficiency	4 %
Trigger efficiency	3 %
<i>Correlated</i>	
L_{int}	3.8 %
$BR(\phi \rightarrow \ell\ell)$	1 %

Table 2: Systematic uncertainties (in percent) contributing to the measurement of the ϕ -meson cross section in pp collisions at $\sqrt{s} = 2.76$ TeV. When the uncertainty values depend on the p_T interval, their minimum and maximum values are quoted.

description of the ALICE $dN_{\text{ch}}/d\eta_{\text{lab}}$ results at mid-rapidity [9]. Averaging over the available p_T range, the discrepancy between the data and the predictions from HIJING and DPMJET amounts to $\sim 18\%$ and $\sim 57\%$, respectively, at backward rapidity (the Pb-going direction) and $\sim 5\%$ and $\sim 9.5\%$, respectively, at forward rapidity (the p-going direction). In all the cases, the generators underestimate the data points.

The ϕ -meson cross section in p-Pb collisions, integrated over the accessible p_T range, $1 < p_T < 7 \text{ GeV}/c$, is shown as a function of rapidity in Fig. 4. The data points, also summarised in Table 4, exhibit a significant asymmetry between the forward and backward rapidity regions. The data point from the ϕ -meson analysis at mid-rapidity in the K^+K^- channel [51], also shown for the $1 < p_T < 7 \text{ GeV}/c$ p_T range, fits well into the trend defined by the two series of points in the backward and forward rapidity regions. This observation complements the previous measurements of light-flavour particle production (charged unidentified particles) reported in p-Pb by ALICE at the LHC at mid-rapidity [9], and in d-Au by PHOBOS at RHIC ranging from mid to forward rapidity [14]. The comparison between the data and the predictions by HIJING and DPMJET, illustrated in Fig. 4, clearly shows how the models — which successfully described charged particle production at mid-rapidity in the same collision system [9] — fail to properly reproduce the shape and the normalisation of the observed rapidity dependence of the ϕ -meson cross section. Still, the HIJING prediction qualitatively reproduces the forward-backward asymmetry observed in the data, as well as — ignoring the normalisation — the shape of the y -dependence in the backward region. DPMJET, on the contrary, fails to reproduce even qualitatively the observed forward-backward asymmetry.

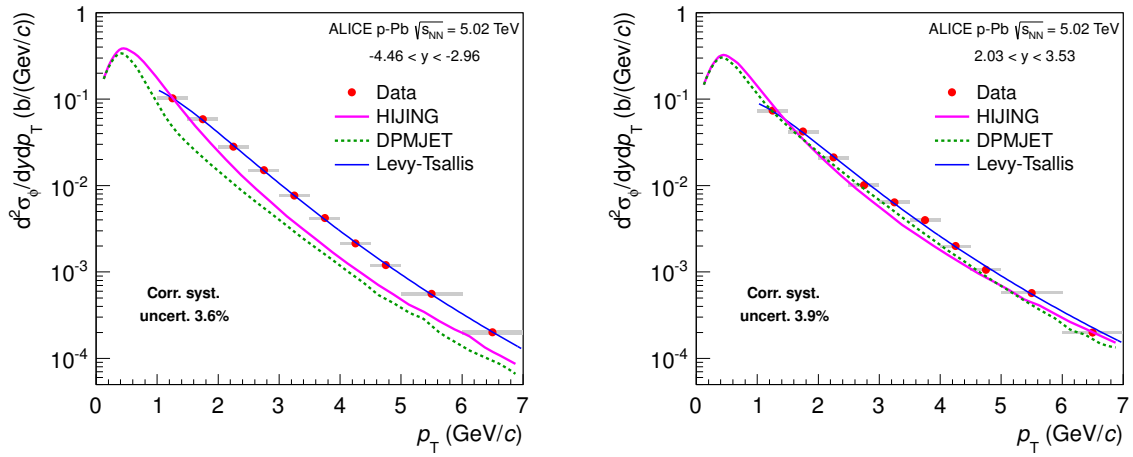


Fig. 3: ϕ -meson cross section in p-Pb collisions at $\sqrt{s_{NN}} = 5.02$ TeV as a function of p_T in the backward (left) and forward (right) rapidity regions. Error bars (smaller than the markers) and boxes represent statistical and systematic uncertainties, respectively. Predictions by HIJING [49] and DPMJET [50] are also shown, together with the result of a fit with the Levy-Tsallis function (Eq. 1).

p_T (GeV/c)	$-4.46 < y < -2.96$		$2.03 < y < 3.53$	
	χ^2/ndf	$d^2\sigma_\phi^{\text{pPb}} / (dy dp_T)$ (mb/(GeV/c))	χ^2/ndf	$d^2\sigma_\phi^{\text{pPb}} / (dy dp_T)$ (mb/(GeV/c))
[1.0, 1.5]	0.7	$102 \pm 8 \pm 12$	1.5	$73.3 \pm 5.6 \pm 8.0$
[1.5, 2.0]	1.2	$58.6 \pm 3.3 \pm 5.5$	1.9	$42.1 \pm 2.5 \pm 4.3$
[2.0, 2.5]	2.5	$28.3 \pm 1.4 \pm 2.9$	1.7	$21.0 \pm 1.2 \pm 2.0$
[2.5, 3.0]	4.2	$15.0 \pm 0.7 \pm 1.2$	3.1	$10.07 \pm 0.77 \pm 0.97$
[3.0, 3.5]	2.6	$7.66 \pm 0.40 \pm 0.70$	2.0	$6.38 \pm 0.41 \pm 0.61$
[3.5, 4.0]	1.9	$4.20 \pm 0.24 \pm 0.34$	1.2	$3.96 \pm 0.30 \pm 0.36$
[4.0, 4.5]	0.7	$2.15 \pm 0.17 \pm 0.16$	1.0	$1.99 \pm 0.20 \pm 0.15$
[4.5, 5.0]	0.9	$1.20 \pm 0.11 \pm 0.10$	0.9	$1.06 \pm 0.13 \pm 0.08$
[5.0, 6.0]	1.0	$0.560 \pm 0.052 \pm 0.054$	1.0	$0.570 \pm 0.088 \pm 0.043$
[6.0, 7.0]	1.2	$0.201 \pm 0.030 \pm 0.028$	0.9	$0.199 \pm 0.045 \pm 0.016$

Table 3: Production cross section for the ϕ -meson in p-Pb collisions at $\sqrt{s_{NN}} = 5.02$ TeV, as a function of p_T , in the backward and forward rapidity regions. The first uncertainty is statistical and the second is the bin-to-bin uncorrelated systematic. The bin-to-bin correlated relative systematic uncertainty is 3.6 % and 3.9 %, respectively, for the backward and the forward regions. The χ^2/ndf values are relative to the hadronic-cocktail fit and the $[0.8, 1.2 \text{ GeV}/c^2]$ mass region.

4.2 Forward-backward ratio in p-Pb collisions

To establish a more direct comparison of the cross section in the p-going and Pb-going directions, σ_ϕ^{pPb} was extracted as a function of p_T in the common $|y|$ range $2.96 < |y| < 3.53$. The p_T interval $1.0 < p_T < 1.5 \text{ GeV}/c$ was discarded in this measurement because of the poor statistics available in this limited rapidity range, resulting in an uncertainty larger than 50 %.

The ratio between the forward and backward cross section, R_{FB} , is shown as a function of p_T in Fig. 5. The data points exhibit no significant p_T dependence within the experimental uncertainties. Predictions by HIJING and DPMJET are also shown, with HIJING slightly overestimating the data points and DPMJET clearly failing to reproduce the observed values, staying above $R_{\text{FB}} = 1$ in the whole p_T range considered here. This observation is consistent with the observations in Fig. 4, where the forward-backward

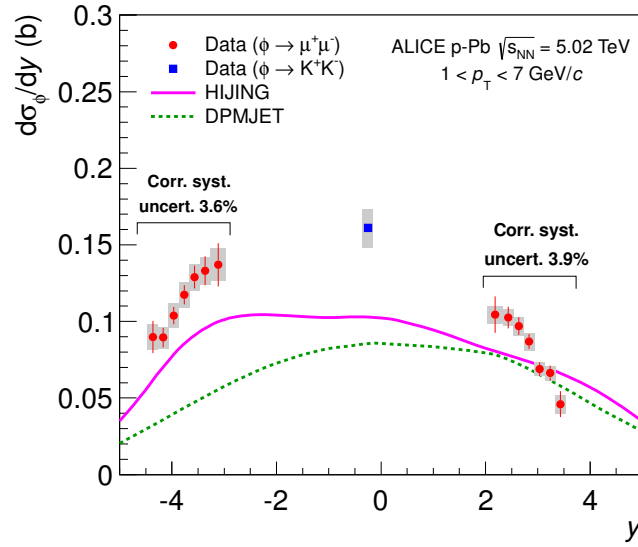


Fig. 4: ϕ -meson cross section in p-Pb collisions at $\sqrt{s_{NN}} = 5.02$ TeV as a function of rapidity, integrated over the range $1 < p_T < 7$ GeV/c. Error bars and boxes represent statistical and systematic uncertainties, respectively. Predictions by HIJING and DPMJET are also shown, together with the mid-rapidity data point from the ϕ -meson measurement in the K^+K^- channel [51], also evaluated in the range $1 < p_T < 7$ GeV/c.

y	χ^2/ndf	$d\sigma_\phi^{\text{pPb}}/dy$ (mb)	y	χ^2/ndf	$d\sigma_\phi^{\text{pPb}}/dy$ (mb)
[-4.46, -4.25]	0.9	$89 \pm 10 \pm 9$	[2.03, 2.35]	2.6	$104 \pm 11 \pm 6$
[-4.25, -4.05]	1.8	$89 \pm 6 \pm 7$	[2.35, 2.55]	1.5	$102 \pm 7 \pm 5$
[-4.05, -3.85]	0.9	$103 \pm 5 \pm 8$	[2.55, 2.75]	2.0	$96 \pm 5 \pm 6$
[-3.85, -3.65]	2.9	$117 \pm 6 \pm 9$	[2.75, 2.95]	1.6	$86 \pm 4 \pm 5$
[-3.65, -3.45]	1.2	$128 \pm 7 \pm 9$	[2.95, 3.15]	2.3	$68 \pm 4 \pm 4$
[-3.45, -3.25]	3.6	$133 \pm 9 \pm 9$	[3.15, 3.35]	1.0	$66 \pm 5 \pm 5$
[-3.25, -2.96]	1.2	$136 \pm 14 \pm 11$	[3.35, 3.53]	1.2	$45 \pm 8 \pm 6$

Table 4: Production cross section for the ϕ -meson in p-Pb collisions at $\sqrt{s_{NN}} = 5.02$ TeV, as a function of rapidity, integrated over the range $1 < p_T < 7$ GeV/c. The first uncertainty is statistical and the second is the bin-to-bin uncorrelated systematic. The bin-to-bin correlated relative systematic uncertainty is 3.6 % and 3.9 %, respectively, for the backward and the forward regions. The χ^2/ndf values are relative to the hadronic-cocktail fit and the [0.8, 1.2 GeV/c²] mass region.

asymmetry of the ϕ -meson yield was better reproduced by HIJING than by DPMJET.

4.3 Nuclear modification factor in p-Pb collisions

The ϕ -meson nuclear modification factor R_{pPb} is defined as the ratio between the production cross section $\sigma_\phi^{\text{pPb}}(p_T)$ in p-Pb collisions and the cross section $\sigma_\phi^{\text{pp}}(p_T)$ in pp collisions — evaluated at $\sqrt{s} = 5.02$ TeV as described in the following — scaled by A_{Pb} :

$$R_{\text{pPb}}(p_T) = \frac{\sigma_\phi^{\text{pPb}}(p_T)}{\sigma_\phi^{\text{pp}}(p_T) \cdot A_{\text{Pb}}}, \quad (2)$$

where A_{Pb} is the nuclear mass number for the Pb nucleus. Since for the pp cross section σ_ϕ^{pp} at $\sqrt{s} = 5.02$ TeV no direct measurement is currently available, it was evaluated by interpolating the measure-

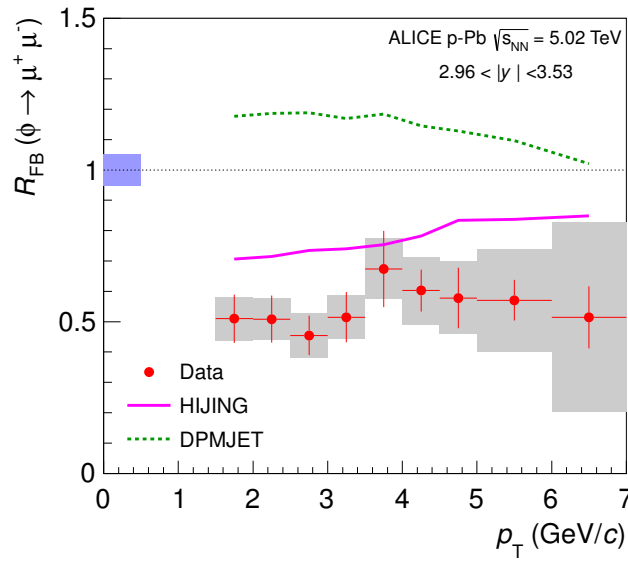


Fig. 5: Forward-backward ratio for the ϕ -meson in p-Pb collisions at $\sqrt{s_{\text{NN}}} = 5.02$ TeV as a function of p_{T} , in the rapidity range $2.96 < |y| < 3.53$ common to the two rapidity regions considered in the analysis. Error bars and boxes represent statistical and systematic uncertainties, respectively. The blue box on the left represents the bin-to-bin correlated systematic uncertainty, see Table 7. Predictions from HIJING and DPMJET are also shown for comparison.

ments in the rapidity interval $2.5 < y < 4$ at $\sqrt{s} = 2.76$ (see Section 4.1.1) and 7 TeV [25]. For each p_{T} interval, the \sqrt{s} dependence of the differential cross section $d^2\sigma_{\phi}^{\text{pp}}/(dydp_{\text{T}})$ was described with a power law $\sigma^{\text{pp}}(\sqrt{s}) = C \cdot (\sqrt{s})^{\alpha}$, where C and α are determined using the data at 2.76 and 7 TeV. Alternative parameterisations were also considered [52], namely a linear and an exponential function, and the mean of the results obtained with the three functions was taken. Since the pp measurements are limited to $1 < p_{\text{T}} < 5$ GeV/c, the cross section at $\sqrt{s_{\text{NN}}} = 5.02$ TeV was extrapolated towards higher p_{T} by means of a Levy-Tsallis function, which describes the calculated differential cross section in the p_{T} range covered by the measurements. The uncertainty on the interpolated cross sections arises from the choice of the function used for the interpolation, from the uncertainties in the measurements at 2.76 and 7 TeV, and — for $p_{\text{T}} > 5$ GeV/c — from the extrapolation based on the Levy-Tsallis fit. They range from about 7% for $p_{\text{T}} = 1$ GeV/c to 20% for $p_{\text{T}} = 5$ GeV/c, and exceed 30% for $p_{\text{T}} > 5$ GeV/c, representing the major source of systematic uncertainty for the measurement of the nuclear modification factor. The interpolated cross section, which refers to the rapidity range $2.5 < y < 4$, was finally scaled to the forward and backward rapidity windows $2.03 < y < 3.53$ and $-4.46 < y < -2.96$, considered for the analysis of the p-Pb data. The relative scaling factors $f_{\text{fwd}} = 1.135 \pm 0.031$ and $f_{\text{bkw}} = 0.850 \pm 0.028$ were evaluated as an average from simulations with PHOJET and the Perugia0, Perugia11, ATLAS-CSC and D6T PYTHIA tunes. In doing so, we also retained the PYTHIA tunes which were observed to fail in describing the pp data (see Section 4.1.1): the reason is that the disagreement between models and data concerns in this case the absolute normalisation more than the shape of the kinematic distributions, which is the only relevant feature in the evaluation of the f_{fwd} and f_{bkw} factors. The uncertainties (amounting to about 3%) correspond to the differences between the considered MC predictions. The numerical values are reported in Table 5.

The nuclear modification factor R_{pPb} as a function of p_{T} is shown in the two panels of Fig. 6 for the backward and forward rapidity regions considered in the analysis. The numerical values are also quoted in Table 6. For each p_{T} interval, the systematic uncertainty detailed in Table 7 results from the quadratic sum of the uncertainty on the ϕ -meson cross section in p-Pb and the one of the pp reference. A rising

p_{T} (GeV/c)	$d^2\sigma_{\phi}/dydp_{\text{T}}$ (mb/(GeV/c))	
	$-4.46 < y < -2.96$	$2.03 < y < 3.53$
[1.0, 1.5]	0.491 ± 0.067	0.656 ± 0.090
[1.5, 2.0]	0.223 ± 0.015	0.297 ± 0.020
[2.0, 2.5]	0.0995 ± 0.0071	0.1328 ± 0.0095
[2.5, 3.0]	0.0467 ± 0.0032	0.0623 ± 0.0043
[3.0, 3.5]	0.0234 ± 0.0015	0.0312 ± 0.0020
[3.5, 4.0]	0.0125 ± 0.0011	0.0167 ± 0.0015
[4.0, 4.5]	0.00706 ± 0.00094	0.0094 ± 0.0012
[4.5, 5.0]	0.00419 ± 0.00082	0.0056 ± 0.0011
[5.0, 6.0]	0.00213 ± 0.00060	0.00284 ± 0.00081
[6.0, 7.0]	0.00093 ± 0.00039	0.00124 ± 0.00052

Table 5: Differential cross section for the ϕ -meson in pp collisions at $\sqrt{s} = 5.02$ TeV in the backward and forward rapidity regions of interest for the analysis of the p-Pb data, as obtained interpolating the available measurements at $\sqrt{s} = 2.76$ and 7 TeV. Total uncertainties, combining statistical and systematic sources, are reported.

trend of R_{pPb} when going from $p_{\text{T}} = 1$ GeV/c to $p_{\text{T}} \approx 3\text{--}4$ GeV/c can be observed both at backward and forward rapidity. The values of R_{pPb} in the two rapidity ranges, however, are significantly different. In particular, at backward rapidity we observe an enhancement of the ϕ -meson cross section with respect to the scaled pp reference peaked around $p_{\text{T}} = 3\text{--}4$ GeV/c. This enhancement, absent in the forward rapidity region, reaches a factor of up to ~ 1.6 and could be associated either to an initial-state effect (including a possible Cronin-like enhancement [4, 53]) or to a final state effect related to radial flow in p-Pb as proposed for recent ALICE measurements at mid-rapidity [12]. Discriminating between these two effects requires more detailed investigations, including differential analyses as a function of global event properties like collision centrality.

Concerning the behaviour at high p_{T} , we observe that the ϕ -meson R_{pPb} is compatible with unity for $p_{\text{T}} \gtrsim 4$ GeV/c in the p-going direction, similar to what was observed for the R_{pPb} of charged particle production at mid-rapidity [10, 12]. The observations in the Pb-going direction do not allow a clear trend of the R_{pPb} factor at high p_{T} to be established. A possible saturation at $R_{\text{pPb}} \approx 1$ for $p_{\text{T}} \gtrsim 5$ GeV/c is, however, still compatible with the measurements.

p_{T} (GeV/c)	R_{pPb}	
	$-4.46 < y < -2.96$	$2.03 < y < 3.53$
[1.0, 1.5]	$1.00 \pm 0.08 \pm 0.18$	$0.537 \pm 0.041 \pm 0.094$
[1.5, 2.0]	$1.26 \pm 0.07 \pm 0.15$	$0.681 \pm 0.040 \pm 0.083$
[2.0, 2.5]	$1.37 \pm 0.07 \pm 0.17$	$0.760 \pm 0.043 \pm 0.091$
[2.5, 3.0]	$1.54 \pm 0.07 \pm 0.16$	$0.777 \pm 0.059 \pm 0.092$
[3.0, 3.5]	$1.57 \pm 0.08 \pm 0.18$	$0.98 \pm 0.06 \pm 0.11$
[3.5, 4.0]	$1.62 \pm 0.09 \pm 0.19$	$1.14 \pm 0.09 \pm 0.15$
[4.0, 4.5]	$1.46 \pm 0.12 \pm 0.22$	$1.02 \pm 0.10 \pm 0.15$
[4.5, 5.0]	$1.38 \pm 0.13 \pm 0.29$	$0.91 \pm 0.11 \pm 0.19$
[5.0, 6.0]	$1.26 \pm 0.12 \pm 0.38$	$0.97 \pm 0.15 \pm 0.29$
[6.0, 7.0]	$1.04 \pm 0.16 \pm 0.46$	$0.77 \pm 0.17 \pm 0.33$

Table 6: Nuclear modification factor R_{pPb} in p-Pb collisions at $\sqrt{s_{\text{NN}}} = 5.02$ TeV for the ϕ -meson as a function of p_{T} in the backward and forward rapidity regions. The first uncertainty is statistical and the second is the bin-to-bin uncorrelated systematic. The bin-to-bin correlated relative systematic uncertainty is 8%.

Source	Syst. uncertainty on $\sigma_{\phi}^{\text{pPb}}$ and R_{pPb}	
	$-4.46 < y < -2.96$	$2.03 < y < 3.53$
<i>Uncorrelated</i>		
Signal extraction	3–5 %	4–8 %
Tracking efficiency	6 %	4 %
Trigger efficiency	3.2 %	2.8 %
$\sigma_{\phi}^{\text{pp}}$	7–30 %	7–30 %
<i>Correlated</i>		
L_{int}	3.5 %	3.8 %
$BR(\phi \rightarrow \ell\ell)$	1 %	1 %
f_{bkw}	3.3 %	—
f_{fwd}	—	2.7 %

Table 7: Systematic uncertainties (in percent) contributing to the measurement of the ϕ -meson cross section and nuclear modification factor in the backward and forward rapidity regions in p-Pb collisions at $\sqrt{s_{\text{NN}}} = 5.02$ TeV. When the uncertainty values depend on the p_{T} interval, their minimum and maximum values are quoted.

Only few other existing measurements can be compared to our data. In particular, results on ϕ -meson production in d-Au collisions at $\sqrt{s_{\text{NN}}} = 200$ GeV have been recently released by the PHENIX Collaboration [54]. The p_{T} -dependence of the R_{dAu} measured by PHENIX, as well as its evolution from backward to forward rapidity, is found to be similar to what is observed in our results for R_{pPb} . Mid-rapidity data on R_{dAu} , also presented by the PHENIX Collaboration for the ϕ -meson, seem to sit between the forward- and backward-rapidity results. Forward-rapidity measurements in d-Au collisions at $\sqrt{s_{\text{NN}}} = 200$ GeV at RHIC [13, 14] are also available for unidentified charged particles, although for the d-going direction only. These data exhibit, similar to our ϕ -meson results in the p-going direction, a rise of R_{dAu} from ~ 0.5 to ~ 1 between $p_{\text{T}} \sim 1$ GeV/ c and $p_{\text{T}} \sim 4$ GeV/ c . A similar rise of R_{pPb} in p-Pb collisions at $\sqrt{s_{\text{NN}}} = 5.02$ TeV is also observed in the already cited measurement of unidentified charged particle and identified charged pion and kaon production at mid-rapidity performed by ALICE [10, 12]. A recent study of ϕ -meson production in p-Pb collisions at mid-rapidity by ALICE [51] does not currently include results on R_{pPb} .

5 Conclusions

We have presented results on ϕ -meson production in the dimuon channel in p-Pb collisions at $\sqrt{s_{\text{NN}}} = 5.02$ TeV obtained by the ALICE experiment at the LHC. Cross section and nuclear modification factor measurements were performed for $1 < p_{\text{T}} < 7$ GeV/ c in the rapidity windows $2.03 < y < 3.53$ (p-going direction) and $-4.46 < y < -2.96$ (Pb-going direction). A corresponding cross section measurement in pp collisions at $\sqrt{s} = 2.76$ TeV has also been reported, for $1 < p_{\text{T}} < 5$ GeV/ c in the region $2.5 < y < 4$. Predictions from HIJING and DPMJET are compared to the p-Pb cross sections and are found to underestimate the data both at backward (by about 18 % and 57 % on average, respectively) and at forward rapidity (by about 5 % and 9.5 % on average, respectively). The forward-backward ratio in the ϕ -meson cross section in p-Pb collisions was measured in the rapidity range $2.96 < |y| < 3.53$, and no significant p_{T} dependence was found within uncertainties. In this case, the data points are significantly overestimated by the DPMJET model, while only a slight disagreement is observed with respect to the HIJING prediction.

In the p-going direction a rising trend of the nuclear modification factor R_{pPb} is observed from ~ 0.5 to ~ 1 , when going from $p_{\text{T}} = 1$ GeV/ c to $p_{\text{T}} = 4$ GeV/ c . This observation is compatible with the behaviour of charged particles at forward rapidity at RHIC energies, and at mid-rapidity at LHC energies. In the

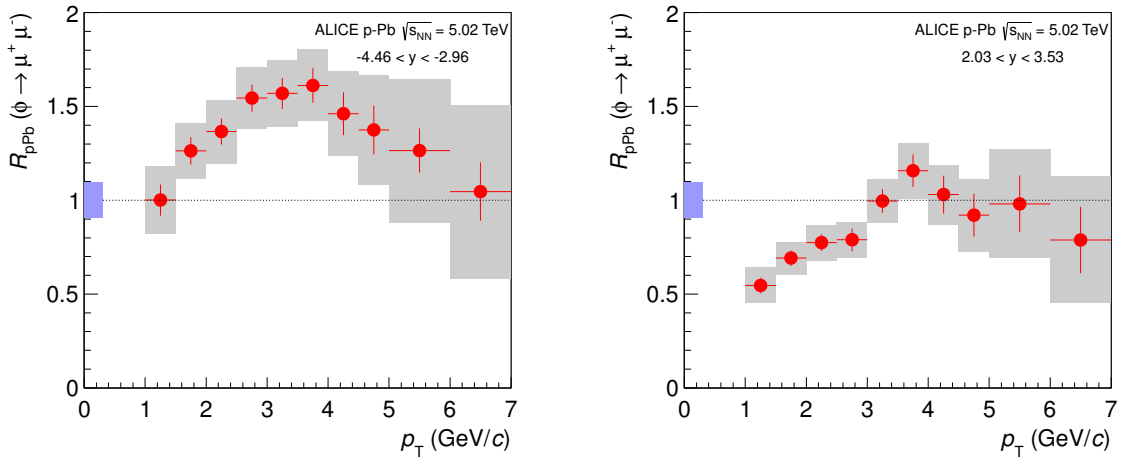


Fig. 6: Nuclear modification factor R_{pPb} in p-Pb collisions at $\sqrt{s_{NN}} = 5.02$ TeV for the ϕ -meson as a function of p_T , in the backward (left) and forward (right) rapidity regions considered in the analysis. Error bars and boxes represent statistical and bin-to-bin uncorrelated systematic uncertainties, respectively. The blue box on the left represents the bin-to-bin correlated systematic uncertainty, see Table 7.

Pb-going direction, on the other hand, an enhancement is observed for R_{pPb} , reaching values as large as ~ 1.6 around $p_T = 3-4$ GeV/c. An interpretation of these results, either in terms of an initial-state (Cronin-like) effect or a final-state effect related to radial flow in p-Pb, is not possible yet, due to a general lack of theoretical predictions for particle production in the light-flavour sector at forward rapidity in p-A collisions at the LHC energies.

Acknowledgements

The ALICE Collaboration would like to thank all its engineers and technicians for their invaluable contributions to the construction of the experiment and the CERN accelerator teams for the outstanding performance of the LHC complex. The ALICE Collaboration gratefully acknowledges the resources and support provided by all Grid centres and the Worldwide LHC Computing Grid (WLCG) collaboration. The ALICE Collaboration acknowledges the following funding agencies for their support in building and running the ALICE detector: State Committee of Science, World Federation of Scientists (WFS) and Swiss Fonds Kidagan, Armenia, Conselho Nacional de Desenvolvimento Científico e Tecnológico (CNPq), Financiadora de Estudos e Projetos (FINEP), Fundação de Amparo à Pesquisa do Estado de São Paulo (FAPESP); National Natural Science Foundation of China (NSFC), the Chinese Ministry of Education (CMOE) and the Ministry of Science and Technology of China (MSTC); Ministry of Education and Youth of the Czech Republic; Danish Natural Science Research Council, the Carlsberg Foundation and the Danish National Research Foundation; The European Research Council under the European Community's Seventh Framework Programme; Helsinki Institute of Physics and the Academy of Finland; French CNRS-IN2P3, the 'Region Pays de Loire', 'Region Alsace', 'Region Auvergne' and CEA, France; German Bundesministerium für Bildung, Wissenschaft, Forschung und Technologie (BMBF) and the Helmholtz Association; General Secretariat for Research and Technology, Ministry of Development, Greece; Hungarian Országos Tudományos Kutatási Alapprogramok (OTKA) and National Office for Research and Technology (NKTH); Department of Atomic Energy and Department of Science and Technology of the Government of India; Istituto Nazionale di Fisica Nucleare (INFN) and Centro Fermi - Museo Storico della Fisica e Centro Studi e Ricerche "Enrico Fermi", Italy; MEXT Grant-in-Aid for Specially Promoted Research, Japan; Joint

Institute for Nuclear Research, Dubna; National Research Foundation of Korea (NRF); Consejo Nacional de Ciencia y Tecnologia (CONACYT), Direccion General de Asuntos del Personal Academico(DGAPA), México, :Amerique Latine Formation academique European Commission(ALFA-EC) and the EPLANET Program (European Particle Physics Latin American Network) Stichting voor Fundamenteel Onderzoek der Materie (FOM) and the Nederlandse Organisatie voor Wetenschappelijk Onderzoek (NWO), Netherlands; Research Council of Norway (NFR); National Science Centre, Poland; Ministry of National Education/Institute for Atomic Physics and Consiliul Naional al Cercetirii tiinifice - Executive Agency for Higher Education Research Development and Innovation Funding (CNCS-UEFISCDI) - Romania; Ministry of Education and Science of Russian Federation, Russian Academy of Sciences, Russian Federal Agency of Atomic Energy, Russian Federal Agency for Science and Innovations and The Russian Foundation for Basic Research; Ministry of Education of Slovakia; Department of Science and Technology, South Africa; Centro de Investigaciones Energeticas, Medioambientales y Tecnologicas (CIEMAT), E-Infrastructure shared between Europe and Latin America (EELA), Ministerio de Economía y Competitividad (MINECO) of Spain, Xunta de Galicia (Consellería de Educación), Centro de Aplicaciones Tecnolgicas y Desarrollo Nuclear (CEADEN), Cubaenergía, Cuba, and IAEA (International Atomic Energy Agency); Swedish Research Council (VR) and Knut & Alice Wallenberg Foundation (KAW); Ukraine Ministry of Education and Science; United Kingdom Science and Technology Facilities Council (STFC); The United States Department of Energy, the United States National Science Foundation, the State of Texas, and the State of Ohio; Ministry of Science, Education and Sports of Croatia and Unity through Knowledge Fund, Croatia. Council of Scientific and Industrial Research (CSIR), New Delhi, India

References

- [1] A. Bazavov, T. Bhattacharya, M. Cheng, C. DeTar, H. Ding, *et al.*, “The chiral and deconfinement aspects of the QCD transition,” *Phys.Rev.* **D85** (2012) 054503, arXiv:1111.1710 [hep-lat].
- [2] **Wuppertal-Budapest** Collaboration, S. Borsanyi *et al.*, “Is there still any T_c mystery in lattice QCD? Results with physical masses in the continuum limit III,” *JHEP* **1009** (2010) 073, arXiv:1005.3508 [hep-lat].
- [3] S. Borsanyi, G. Endrodi, Z. Fodor, A. Jakovac, S. D. Katz, *et al.*, “The QCD equation of state with dynamical quarks,” *JHEP* **1011** (2010) 077, arXiv:1007.2580 [hep-lat].
- [4] A. Accardi, “Cronin effect in proton nucleus collisions: A Survey of theoretical models,” arXiv:hep-ph/0212148 [hep-ph].
- [5] C. Salgado, J. Alvarez-Muniz, F. Arleo, N. Armesto, M. Botje, *et al.*, “Proton-Nucleus Collisions at the LHC: Scientific Opportunities and Requirements,” *J.Phys.* **G39** (2012) 015010, arXiv:1105.3919 [hep-ph].
- [6] M. Brandt, M. Klasen, and F. Knig, “Nuclear parton density modifications from low-mass lepton pair production at the LHC,” *Nucl. Phys.* **A927** (2014) 78–90, arXiv:1401.6817 [hep-ph].
- [7] **BRAHMS** Collaboration, I. Arsene *et al.*, “Quark gluon plasma and color glass condensate at RHIC? The Perspective from the BRAHMS experiment,” *Nucl.Phys.* **A757** (2005) 1–27, arXiv:nucl-ex/0410020 [nucl-ex].
- [8] B. Back, M. Baker, M. Ballintijn, D. Barton, B. Becker, *et al.*, “The PHOBOS perspective on discoveries at RHIC,” *Nucl.Phys.* **A757** (2005) 28–101, arXiv:nucl-ex/0410022 [nucl-ex].
- [9] **ALICE** Collaboration, B. Abelev *et al.*, “Pseudorapidity density of charged particles p-Pb collisions at $\sqrt{s_{NN}} = 5.02$ TeV,” *Phys.Rev.Lett.* **110** (2013) 032301, arXiv:1210.3615 [nucl-ex].

- [10] **ALICE** Collaboration, B. Abelev *et al.*, “Transverse Momentum Distribution and Nuclear Modification Factor of Charged Particles in p-Pb Collisions at $\sqrt{s_{NN}} = 5.02$ TeV,” *Phys.Rev.Lett.* **110** (2013) 082302, arXiv:1210.4520 [nucl-ex].
- [11] **ALICE** Collaboration, B. Abelev *et al.*, “Transverse momentum dependence of inclusive primary charged-particle production in p-Pb collisions at $\sqrt{s_{NN}} = 5.02$ TeV,” *Eur.Phys.J.* **C74** no. 9, (2014) 3054, arXiv:1405.2737 [nucl-ex].
- [12] **ALICE** Collaboration, J. Adam *et al.*, “Multiplicity dependence of charged pion, kaon, and (anti)proton production at large transverse momentum in p-Pb collisions at $\sqrt{s_{NN}} = 5.02$ TeV,” *Phys. Lett.* **B760** (2016) 720–735, arXiv:1601.03658 [nucl-ex].
- [13] **BRAHMS** Collaboration, I. Arsene *et al.*, “On the evolution of the nuclear modification factors with rapidity and centrality in d + Au collisions at $\sqrt{s_{NN}} = 200$ GeV,” *Phys.Rev.Lett.* **93** (2004) 242303, arXiv:nucl-ex/0403005 [nucl-ex].
- [14] **PHOBOS** Collaboration, B. Back *et al.*, “Pseudorapidity distribution of charged particles in d + Au collisions at $\sqrt{s_{NN}} = 200$ GeV,” *Phys.Rev.Lett.* **93** (2004) 082301, arXiv:nucl-ex/0311009 [nucl-ex].
- [15] J. Rafelski and B. Muller, “Strangeness Production in the Quark - Gluon Plasma,” *Phys.Rev.Lett.* **48** (1982) 1066.
- [16] A. Shor, “ ϕ -meson production as a probe of the Quark Gluon Plasma,” *Phys.Rev.Lett.* **54** (1985) 1122–1125.
- [17] P. Koch, B. Muller, and J. Rafelski, “Strangeness in Relativistic Heavy Ion Collisions,” *Phys.Rept.* **142** (1986) 167–262.
- [18] **NA49** Collaboration, C. Alt *et al.*, “System-size dependence of strangeness production in nucleus-nucleus collisions at $s(NN)^{1/2} = 17.3$ -GeV,” *Phys. Rev. Lett.* **94** (2005) 052301, arXiv:nucl-ex/0406031 [nucl-ex].
- [19] **NA49** Collaboration, C. Alt *et al.*, “Energy dependence of phi meson production in central Pb+Pb collisions at $s(NN)^{1/2} = 6$ to 17 GeV,” *Phys. Rev.* **C78** (2008) 044907, arXiv:0806.1937 [nucl-ex].
- [20] **NA50** Collaboration, B. Alessandro *et al.*, “phi production in Pb - Pb collisions at 158-GeV/c per nucleon incident momentum,” *Phys. Lett.* **B555** (2003) 147–155. [Erratum: *Phys. Lett.* **B561**,294(2003)].
- [21] **NA60** Collaboration, K. Banicz *et al.*, “phi Production in In-In Collisions at 158-A-GeV,” *Eur. Phys. J.* **C64** (2009) 1–18, arXiv:0906.1102 [hep-ex].
- [22] **NA60** Collaboration, R. Arnaldi *et al.*, “A Comparative measurement of $\phi \rightarrow K^+K^-$ and $\phi \rightarrow \mu^+\mu^-$ in In-In collisions at the CERN SPS,” *Phys. Lett.* **B699** (2011) 325–329, arXiv:1104.4060 [nucl-ex].
- [23] **STAR** Collaboration, B. Abelev *et al.*, “Measurements of phi meson production in relativistic heavy-ion collisions at RHIC,” *Phys. Rev.* **C79** (2009) 064903, arXiv:0809.4737 [nucl-ex].
- [24] **PHENIX** Collaboration, S. S. Adler *et al.*, “Production of phi mesons at mid-rapidity in $s(NN)^{1/2} = 200$ - GeV Au+Au collisions at RHIC,” *Phys. Rev.* **C72** (2005) 014903, arXiv:nucl-ex/0410012 [nucl-ex].

- [25] ALICE Collaboration, B. Abelev *et al.*, “Light vector meson production in pp collisions at $\sqrt{s} = 7$ TeV,” *Phys.Lett.* **B710** (2012) 557–568, arXiv:1112.2222 [nucl-ex].
- [26] ALICE Collaboration, K. Aamodt *et al.*, “The ALICE experiment at the CERN LHC,” *JINST* **3** (2008) S08002.
- [27] ALICE Collaboration, B. Abelev *et al.*, “Performance of the ALICE Experiment at the CERN LHC,” *Int.J.Mod.Phys.* **A29** (2014) 1430044, arXiv:1402.4476 [nucl-ex].
- [28] ALICE Collaboration, M. Gagliardi, “Measurement of reference cross sections in pp and Pb-Pb collisions at the LHC in van der Meer scans with the ALICE detector,” *AIP Conf.Proc.* **1422** (2012) 110–116, arXiv:1109.5369 [hep-ex].
- [29] ALICE Collaboration, B. Abelev *et al.*, “ J/ψ production and nuclear effects in p-Pb collisions at $\sqrt{s_{NN}} = 5.02$ TeV,” *JHEP* **1402** (2014) 073, arXiv:1308.6726 [nucl-ex].
- [30] ALICE Collaboration, B. Abelev *et al.*, “Measurement of visible cross sections in proton-lead collisions at $\sqrt{s_{NN}} = 5.02$ TeV in van der Meer scans with the ALICE detector,” *JINST* **9** no. 11, (2014) P11003, arXiv:1405.1849 [nucl-ex].
- [31] ALICE Collaboration, B. Abelev *et al.*, “Measurement of quarkonium production at forward rapidity in pp collisions at $\sqrt{s} = 7$ TeV,” *Eur.Phys.J.* **C74** no. 8, (2014) 2974, arXiv:1403.3648 [nucl-ex].
- [32] ALICE Collaboration, B. Abelev *et al.*, “Measurement of inelastic, single- and double-diffraction cross sections in proton–proton collisions at the LHC with ALICE,” *Eur.Phys.J.* **C73** no. 6, (2013) 2456, arXiv:1208.4968 [hep-ex].
- [33] ALICE Collaboration, L. Aphenche *et al.*, “Numerical Simulations and Offline Reconstruction of the Muon Spectrometer of ALICE, ALICE-INT-2009-044,”.
- [34] ALICE Collaboration, G. Chabratova *et al.*, “Development of the Kalman filter for tracking in the forward muon spectrometer of ALICE, ALICE-INT-2003-002,”.
- [35] ALICE Collaboration, “Supplemental figures for “ ϕ -meson production at forward rapidity in p-Pb collisions at $\sqrt{s_{NN}} = 5.02$ TeV and in pp collisions at $\sqrt{s} = 2.76$ TeV”,”. <https://cds.cern.ch/record/2195308>.
- [36] T. Sjostrand, S. Mrenna, and P. Z. Skands, “PYTHIA 6.4 Physics and Manual,” *JHEP* **0605** (2006) 026, arXiv:hep-ph/0603175 [hep-ph].
- [37] R. Brun, F. Carminati, and S. Giani, “GEANT Detector Description and Simulation Tool, CERN-W-5013, 1994,”.
- [38] Particle Data Group Collaboration, J. Beringer *et al.*, “Review of Particle Physics (RPP),” *Phys.Rev.* **D86** (2012) 010001.
- [39] M. Oreglia, *A Study of the Reactions $\psi' \rightarrow \gamma\gamma\psi$* . PhD thesis, SLAC, 1980. <http://search.proquest.com/docview/303036283>.
- [40] ALICE Collaboration, K. Aamodt *et al.*, “Rapidity and transverse momentum dependence of inclusive J/ψ production in pp collisions at $\sqrt{s} = 7$ TeV,” *Phys. Lett.* **B704** (2011) 442–455, arXiv:1105.0380 [hep-ex]. [Erratum: *Phys. Lett.* **B718,692**(2012)].
- [41] R. Barlow, “Systematic errors: Facts and fictions,” arXiv:hep-ex/0207026 [hep-ex].

- [42] R. Engel and J. Ranft, “Hadronic photon-photon interactions at high-energies,” *Phys.Rev.* **D54** (1996) 4244–4262, arXiv:hep-ph/9509373 [hep-ph].
- [43] P. Z. Skands, “Tuning Monte Carlo Generators: The Perugia Tunes,” *Phys.Rev.* **D82** (2010) 074018, arXiv:1005.3457 [hep-ph].
- [44] C. Buttar, D. Clements, I. Dawson, and A. Moraes, “Simulations of minimum bias events and the underlying event, MC tuning and predictions for the LHC,” *Acta Phys.Polon.* **B35** (2004) 433–441.
- [45] R. Field, “Physics at the Tevatron,” *Acta Phys.Polon.* **B39** (2008) 2611–2672.
- [46] ALICE Collaboration, B. Abelev *et al.*, “Production of $K^*(892)^0$ and $\phi(1020)$ in pp collisions at $\sqrt{s} = 7$ TeV,” *Eur.Phys.J.* **C72** (2012) 2183, arXiv:1208.5717 [hep-ex].
- [47] CMS Collaboration, S. Chatrchyan *et al.*, “Study of the inclusive production of charged pions, kaons, and protons in pp collisions at $\sqrt{s} = 0.9, 2.76,$ and 7 TeV,” *Eur.Phys.J.* **C72** (2012) 2164, arXiv:1207.4724 [hep-ex].
- [48] C. Tsallis, “Possible Generalization of Boltzmann-Gibbs Statistics,” *J.Statist.Phys.* **52** (1988) 479–487.
- [49] X.-N. Wang and M. Gyulassy, “HIJING: A Monte Carlo model for multiple jet production in p p, p A and A A collisions,” *Phys.Rev.* **D44** (1991) 3501–3516.
- [50] S. Roesler, R. Engel, and J. Ranft, “The Monte Carlo event generator DPMJET-III,” in *Advanced Monte Carlo for radiation physics, particle transport simulation and applications. Proceedings, Conference, MC2000, Lisbon, Portugal, October 23-26, 2000*, pp. 1033–1038. 2000. arXiv:hep-ph/0012252 [hep-ph]. <http://www-public.slac.stanford.edu/sciDoc/docMeta.aspx?slacPubNumber=SLAC-PUB-8740>.
- [51] ALICE Collaboration, J. Adam *et al.*, “Production of $K^*(892)^0$ and $\phi(1020)$ in p-Pb collisions at $\sqrt{s_{NN}} = 5.02$ TeV,” *Eur. Phys. J.* **C76** no. 5, (2016) 245, arXiv:1601.07868 [nucl-ex].
- [52] ALICE, LHCb Collaboration, “Reference pp cross-sections for J/ψ studies in proton-lead collisions at $\sqrt{s_{NN}} = 5.02$ TeV and comparisons between ALICE and LHCb results,” <http://cds.cern.ch/record/1639617>. CONF-2013-013.
- [53] HERA-B Collaboration, I. Abt *et al.*, “ K^*0 and phi meson production in proton-nucleus interactions at $s^{*(1/2)} = 41.6$ -GeV,” *Eur.Phys.J.* **C50** (2007) 315–328, arXiv:hep-ex/0606049 [hep-ex].
- [54] PHENIX Collaboration, A. Adare *et al.*, “ ϕ meson production in d +Au collisions at $\sqrt{s_{NN}} = 200$ GeV,” *Phys. Rev.* **C92** no. 4, (2015) 044909, arXiv:1506.08181 [nucl-ex].

A The ALICE Collaboration

J. Adam⁴⁰, D. Adamová⁸³, M.M. Aggarwal⁸⁷, G. Aglieri Rinella³⁶, M. Agnello¹¹¹, N. Agrawal⁴⁸, Z. Ahammed¹³², S.U. Ahn⁶⁸, I. Aimo^{94,111}, S. Aiola¹³⁶, M. Ajaz¹⁶, A. Akimov⁵⁸, S.N. Alam¹³², D. Aleksandrov¹⁰⁰, B. Alessandro¹¹¹, D. Alexandre¹⁰², R. Alfaro Molina⁶⁴, A. Alici^{105,12}, A. Alkin³, J.R.M. Almaraz¹¹⁹, J. Alme³⁸, T. Alt⁴³, S. Altinpinar¹⁸, I. Altsybeev¹³¹, C. Alves Garcia Prado¹²⁰, C. Andrei⁷⁸, A. Andronic⁹⁷, V. Anguelov⁹³, J. Anielski⁵⁴, T. Antičić⁹⁸, F. Antinori¹⁰⁸, P. Antonioli¹⁰⁵, L. Aphecetche¹¹³, H. Appelshäuser⁵³, S. Arcelli²⁸, N. Armesto¹⁷, R. Arnaldi¹¹¹, I.C. Arsene²², M. Arslandok⁵³, B. Audurier¹¹³, A. Augustinus³⁶, R. Averbeck⁹⁷, M.D. Azmi¹⁹, M. Bach⁴³, A. Badalà¹⁰⁷, Y.W. Baek⁴⁴, S. Bagnasco¹¹¹, R. Bailhache⁵³, R. Bala⁹⁰, A. Baldisseri¹⁵, F. Baltasar Dos Santos Pedrosa³⁶, R.C. Baral⁶¹, A.M. Barbano¹¹¹, R. Barbera²⁹, F. Barile³³, G.G. Barnaföldi¹³⁵, L.S. Barnby¹⁰², V. Barret⁷⁰, P. Bartalini⁷, K. Barth³⁶, J. Bartke¹¹⁷, E. Bartsch⁵³, M. Basile²⁸, N. Bastid⁷⁰, S. Basu¹³², B. Bathen⁵⁴, G. Batigne¹¹³, A. Batista Camejo⁷⁰, B. Batyunya⁶⁶, P.C. Batzing²², I.G. Bearden⁸⁰, H. Beck⁵³, C. Bedda¹¹¹, N.K. Behera^{48,49}, I. Belikov⁵⁵, F. Bellini²⁸, H. Bello Martinez², R. Bellwied¹²², R. Belmont¹³⁴, E. Belmont-Moreno⁶⁴, V. Belyaev⁷⁶, G. Bencedi¹³⁵, S. Beole²⁷, I. Berceanu⁷⁸, A. Bercuci⁷⁸, Y. Berdnikov⁸⁵, D. Berenyi¹³⁵, R.A. Bertens⁵⁷, D. Berzano^{36,27}, L. Betev³⁶, A. Bhasin⁹⁰, I.R. Bhat⁹⁰, A.K. Bhati⁸⁷, B. Bhattacharjee⁴⁵, J. Bhom¹²⁸, L. Bianchi¹²², N. Bianchi⁷², C. Bianchin^{134,57}, J. Bielčik⁴⁰, J. Bielčíková⁸³, A. Bilandzic⁸⁰, R. Biswas⁴, S. Biswas⁷⁹, S. Bjelogrić⁵⁷, J.T. Blair¹¹⁸, F. Blanco¹⁰, D. Blau¹⁰⁰, C. Blume⁵³, F. Bock^{93,74}, A. Bogdanov⁷⁶, H. Bøggild⁸⁰, L. Boldizsár¹³⁵, M. Bombara⁴¹, J. Book⁵³, H. Borel¹⁵, A. Borissov⁹⁶, M. Borri⁸², F. Bossu⁶⁵, E. Botta²⁷, S. Böttger⁵², P. Braun-Munzinger⁹⁷, M. Bregant¹²⁰, T. Breitner⁵², T.A. Brooker⁵³, T.A. Browning⁹⁵, M. Broz⁴⁰, E.J. Brucken⁴⁶, E. Bruna¹¹¹, G.E. Bruno³³, D. Budnikov⁹⁹, H. Buesching⁵³, S. Bufalino^{27,111}, P. Buncic³⁶, O. Busch^{128,93}, Z. Buthelezi⁶⁵, J.B. Butt¹⁶, J.T. Buxton²⁰, D. Caffarri³⁶, X. Cai⁷, H. Caines¹³⁶, L. Calero Diaz⁷², A. Caliva⁵⁷, E. Calvo Villar¹⁰³, P. Camerini²⁶, F. Carena³⁶, W. Carena³⁶, F. Carnesecchi²⁸, J. Castillo Castellanos¹⁵, A.J. Castro¹²⁵, E.A.R. Casula²⁵, C. Cavicchioli³⁶, C. Ceballos Sanchez⁹, J. Cepila⁴⁰, P. Cerello¹¹¹, J. Cercala¹¹⁵, B. Chang¹²³, S. Chapeland³⁶, M. Chartier¹²⁴, J.L. Charvet¹⁵, S. Chattopadhyay¹³², S. Chattopadhyay¹⁰¹, V. Chelnokov³, M. Cherney⁸⁶, C. Cheshkov¹³⁰, B. Cheynis¹³⁰, V. Chibante Barroso³⁶, D.D. Chinellato¹²¹, P. Chochula³⁶, K. Choi⁹⁶, M. Chojnacki⁸⁰, S. Choudhury¹³², P. Christakoglou⁸¹, C.H. Christensen⁸⁰, P. Christiansen³⁴, T. Chujo¹²⁸, S.U. Chung⁹⁶, Z. Chuhui⁵⁷, C. Cicalo¹⁰⁶, L. Cifarelli^{12,28}, F. Cindolo¹⁰⁵, J. Cleymans⁸⁹, F. Colamaria³³, D. Colella^{36,33,59}, A. Collu²⁵, M. Colocci²⁸, G. Conesa Balbastre⁷¹, Z. Conesa del Valle⁵¹, M.E. Connors¹³⁶, J.G. Contreras^{11,40}, T.M. Cormier⁸⁴, Y. Corrales Morales²⁷, I. Cortés Maldonado², P. Cortese³², M.R. Cosentino¹²⁰, F. Costa³⁶, P. Crochet⁷⁰, R. Cruz Albino¹¹, E. Cuautle⁶³, L. Cunqueiro³⁶, T. Dahms^{92,37}, A. Dainese¹⁰⁸, A. Danu⁶², D. Das¹⁰¹, I. Das^{101,51}, S. Das⁴, A. Dash¹²¹, S. Dash⁴⁸, S. De¹²⁰, A. De Caro^{31,12}, G. de Cataldo¹⁰⁴, J. de Cuveland⁴³, A. De Falco²⁵, D. De Gruttola^{12,31}, N. De Marco¹¹¹, S. De Pasquale³¹, A. Deisting^{97,93}, A. Deloff⁷⁷, E. Dénes^{135,i}, G. D'Erasmus³³, D. Di Bari³³, A. Di Mauro³⁶, P. Di Nezza⁷², M.A. Diaz Corchero¹⁰, T. Dietel⁸⁹, P. Dillenseger⁵³, R. Divi³⁶, Ø. Djuvsland¹⁸, A. Dobrin^{57,81}, T. Dobrowolski^{77,i}, D. Domenicis Gimenez¹²⁰, B. Dönigus⁵³, O. Dordic²², T. Drozhzhova⁵³, A.K. Dubey¹³², A. Dubla⁵⁷, L. Ducroux¹³⁰, P. Dupieux⁷⁰, R.J. Ehlers¹³⁶, D. Elia¹⁰⁴, H. Engel⁵², B. Erasmus^{36,113}, I. Erdemir⁵³, F. Erhardt¹²⁹, D. Eschweiler⁴³, B. Espagnon⁵¹, M. Estienne¹¹³, S. Esumi¹²⁸, J. Eum⁹⁶, D. Evans¹⁰², S. Evdokimov¹¹², G. Eyyubova⁴⁰, L. Fabbietti^{37,92}, D. Fabris¹⁰⁸, J. Faivre⁷¹, A. Fantoni⁷², M. Fasel⁷⁴, L. Feldkamp⁵⁴, D. Felea⁶², A. Feliciello¹¹¹, G. Feofilov¹³¹, J. Ferencei⁸³, A. Fernández Téllez², E.G. Ferreira¹⁷, A. Ferretti²⁷, A. Festanti³⁰, V.J.G. Feuillard^{15,70}, J. Figiel¹¹⁷, M.A.S. Figueredo^{124,120}, S. Filchagin⁹⁹, D. Finogeev⁵⁶, F.M. Fionda²⁵, E.M. Fiore³³, M.G. Fleck⁹³, M. Floris³⁶, S. Foertsch⁶⁵, P. Foka⁹⁷, S. Fokin¹⁰⁰, E. Fragiacomo¹¹⁰, A. Francescon^{36,30}, U. Frankenfeld⁹⁷, U. Fuchs³⁶, C. Furget⁷¹, A. Furs⁵⁶, M. Fusco Girard³¹, J.J. Gaardhøje⁸⁰, M. Gagliardi²⁷, A.M. Gago¹⁰³, M. Gallio²⁷, D.R. Gangadharan⁷⁴, P. Ganoti⁸⁸, C. Gao⁷, C. Garabatos⁹⁷, E. Garcia-Solis¹³, C. Gargiulo³⁶, P. Gasik^{92,37}, M. Germain¹¹³, A. Gheata³⁶, M. Gheata³⁶, P. Ghosh¹³², S.K. Ghosh⁴, P. Gianotti⁷², P. Giubellino^{36,111}, P. Giubilato³⁰, E. Gladysz-Dziadus¹¹⁷, P. Glässel⁹³, D.M. Gómez Coral⁶⁴, A. Gomez Ramirez⁵², P. González-Zamora¹⁰, S. Gorbunov⁴³, L. Görlich¹¹⁷, S. Gotovac¹¹⁶, V. Grabski⁶⁴, L.K. Graczykowski¹³³, K.L. Graham¹⁰², A. Grelli⁵⁷, A. Grigoras³⁶, C. Grigoras³⁶, V. Grigoriev⁷⁶, A. Grigoryan¹, S. Grigoryan⁶⁶, B. Grinyov³, N. Grion¹¹⁰, J.F. Grosse-Oetringhaus³⁶, J.-Y. Grossiord¹³⁰, R. Grosso³⁶, F. Guber⁵⁶, R. Guernane⁷¹, B. Guerzoni²⁸, K. Gulbrandsen⁸⁰, H. Gulkanyan¹, T. Gunji¹²⁷, A. Gupta⁹⁰, R. Gupta⁹⁰, R. Haake⁵⁴, Ø. Haaland¹⁸, C. Hadjidakis⁵¹, M. Haiduc⁶², H. Hamagaki¹²⁷, G. Hamar¹³⁵, A. Hansen⁸⁰, J.W. Harris¹³⁶, H. Hartmann⁴³, A. Harton¹³, D. Hatzifotiadou¹⁰⁵, S. Hayashi¹²⁷, S.T. Heckel⁵³, M. Heide⁵⁴, H. Helstrup³⁸, A. Herghelegiu⁷⁸, G. Herrera Corral¹¹, B.A. Hess³⁵, K.F. Hetland³⁸, T.E. Hilden⁴⁶, H. Hillemanns³⁶, B. Hippolyte⁵⁵, R. Hosokawa¹²⁸, P. Hristov³⁶, M. Huang¹⁸, T.J. Humanic²⁰, N. Hussain⁴⁵, T. Hussain¹⁹, D. Hutter⁴³, D.S. Hwang²¹, R. Ilkaev⁹⁹, I. Ilkiv⁷⁷, M. Inaba¹²⁸,

M. Ippolitov^{76,100}, M. Irfan¹⁹, M. Ivanov⁹⁷, V. Ivanov⁸⁵, V. Izucheev¹¹², P.M. Jacobs⁷⁴, S. Jadlovská¹¹⁵, C. Jahnke¹²⁰, H.J. Jang⁶⁸, M.A. Janik¹³³, P.H.S.Y. Jayarathna¹²², C. Jena³⁰, S. Jena¹²², R.T. Jimenez Bustamante⁹⁷, P.G. Jones¹⁰², H. Jung⁴⁴, A. Jusko¹⁰², P. Kalinak⁵⁹, A. Kalweit³⁶, J. Kamin⁵³, J.H. Kang¹³⁷, V. Kaplin⁷⁶, S. Kar¹³², A. Karasu Uysal⁶⁹, O. Karavichev⁵⁶, T. Karavicheva⁵⁶, L. Karayan^{93,97}, E. Karpechev⁵⁶, U. Kebschull⁵², R. Keidel¹³⁸, D.L.D. Keijdener⁵⁷, M. Keil³⁶, K.H. Khan¹⁶, M.M. Khan¹⁹, P. Khan¹⁰¹, S.A. Khan¹³², A. Khanzadeev⁸⁵, Y. Kharlov¹¹², B. Kileng³⁸, B. Kim¹³⁷, D.W. Kim^{44,68}, D.J. Kim¹²³, H. Kim¹³⁷, J.S. Kim⁴⁴, M. Kim⁴⁴, M. Kim¹³⁷, S. Kim²¹, T. Kim¹³⁷, S. Kirsch⁴³, I. Kisel⁴³, S. Kiselev⁵⁸, A. Kisiel¹³³, G. Kiss¹³⁵, J.L. Klay⁶, C. Klein⁵³, J. Klein^{36,93}, C. Klein-Bösing⁵⁴, A. Kluge³⁶, M.L. Knichel⁹³, A.G. Knospe¹¹⁸, T. Kobayashi¹²⁸, C. Kobdaj¹¹⁴, M. Kofarago³⁶, T. Kollegger^{97,43}, A. Kolojvari¹³¹, V. Kondratiev¹³¹, N. Kondratyeva⁷⁶, E. Kondratyuk¹¹², A. Konevskikh⁵⁶, M. Kopcik¹¹⁵, M. Kour⁹⁰, C. Kouzinopoulos³⁶, O. Kovalenko⁷⁷, V. Kovalenko¹³¹, M. Kowalski¹¹⁷, G. Koyithatta Meethalevedu⁴⁸, J. Kral¹²³, I. Králik⁵⁹, A. Kravčáková⁴¹, M. Kretz⁴³, M. Krivda^{59,102}, F. Krizek⁸³, E. Kryshen³⁶, M. Krzewicki⁴³, A.M. Kubera²⁰, V. Kučera⁸³, T. Kugathasan³⁶, C. Kuhn⁵⁵, P.G. Kuijer⁸¹, A. Kumar⁹⁰, J. Kumar⁴⁸, L. Kumar^{79,87}, P. Kurashvili⁷⁷, A. Kurepin⁵⁶, A.B. Kurepin⁵⁶, A. Kuryakin⁹⁹, S. Kuschpil⁸³, M.J. Kweon⁵⁰, Y. Kwon¹³⁷, S.L. La Pointe¹¹¹, P. La Rocca²⁹, C. Lagana Fernandes¹²⁰, I. Lakomov³⁶, R. Langoy⁴², C. Lara⁵², A. Lardeux¹⁵, A. Lattuca²⁷, E. Laudi³⁶, R. Lea²⁶, L. Leardini⁹³, G.R. Lee¹⁰², S. Lee¹³⁷, I. Légrand³⁶, F. Lehas⁸¹, R.C. Lemmon⁸², V. Lenti¹⁰⁴, E. Leogrande⁵⁷, I. León Monzón¹¹⁹, M. Leoncino²⁷, P. Lévai¹³⁵, S. Li^{7,70}, X. Li¹⁴, J. Lien⁴², R. Lietava¹⁰², S. Lindal²², V. Lindenstruth⁴³, C. Lippmann⁹⁷, M.A. Lisa²⁰, H.M. Ljunggren³⁴, D.F. Lodato⁵⁷, P.I. Loenne¹⁸, V. Loginov⁷⁶, C. Loizides⁷⁴, X. Lopez⁷⁰, E. López Torres⁹, A. Lowe¹³⁵, P. Luettig⁵³, M. Lunardon³⁰, G. Luparello²⁶, P.H.F.N.D. Luz¹²⁰, A. Maevskaya⁵⁶, M. Mager³⁶, S. Mahajan⁹⁰, S.M. Mahmood²², A. Maire⁵⁵, R.D. Majka¹³⁶, M. Malaev⁸⁵, I. Maldonado Cervantes⁶³, L. Malinina^{ii,66}, D. Mal'Kevich⁵⁸, P. Malzacher⁹⁷, A. Mamonov⁹⁹, V. Manko¹⁰⁰, F. Manso⁷⁰, V. Manzari^{36,104}, M. Marchisone²⁷, J. Mareš⁶⁰, G.V. Margagliotti²⁶, A. Margotti¹⁰⁵, J. Margutti⁵⁷, A. Marín⁹⁷, C. Markert¹¹⁸, M. Marquard⁵³, N.A. Martin⁹⁷, J. Martin Blanco¹¹³, P. Martinengo³⁶, M.I. Martínez², G. Martínez García¹¹³, M. Martinez Pedreira³⁶, Y. Martynov³, A. Mas¹²⁰, S. Masciocchi⁹⁷, M. Masera²⁷, A. Masoni¹⁰⁶, L. Massacrier¹¹³, A. Mastroserio³³, H. Masui¹²⁸, A. Matyjka¹¹⁷, C. Mayer¹¹⁷, J. Mazer¹²⁵, M.A. Mazzoni¹⁰⁹, D. McDonald¹²², F. Meddi²⁴, Y. Melikyan⁷⁶, A. Menchaca-Rocha⁶⁴, E. Meninno³¹, J. Mercado Pérez⁹³, M. Meres³⁹, Y. Miake¹²⁸, M.M. Mieskolainen⁴⁶, K. Mikhaylov^{66,58}, L. Milano³⁶, J. Milosevic²², L.M. Minervini^{104,23}, A. Mischke⁵⁷, A.N. Mishra⁴⁹, D. Miśkowiec⁹⁷, J. Mitra¹³², C.M. Mitu⁶², N. Mohammadi⁵⁷, B. Mohanty^{132,79}, L. Molnar⁵⁵, L. Montaño Zetina¹¹, E. Montes¹⁰, M. Morando³⁰, D.A. Moreira De Godoy^{113,54}, S. Moretto³⁰, A. Morreale¹¹³, A. Morsch³⁶, V. Muccifora⁷², E. Mudnic¹¹⁶, D. Mühlheim⁵⁴, S. Muhuri¹³², M. Mukherjee¹³², J.D. Mulligan¹³⁶, M.G. Munhoz¹²⁰, S. Murray⁶⁵, L. Musa³⁶, J. Musinsky⁵⁹, B.K. Nandi⁴⁸, R. Nania¹⁰⁵, E. Nappi¹⁰⁴, M.U. Naru¹⁶, C. Natrass¹²⁵, K. Nayak⁷⁹, T.K. Nayak¹³², S. Nazarenko⁹⁹, A. Nedosekin⁵⁸, L. Nellen⁶³, F. Ng¹²², M. Nicassio⁹⁷, M. Niculescu^{62,36}, J. Niedziela³⁶, B.S. Nielsen⁸⁰, S. Nikolaev¹⁰⁰, S. Nikulin¹⁰⁰, V. Nikulin⁸⁵, F. Noferini^{105,12}, P. Nomokonov⁶⁶, G. Nooren⁵⁷, J.C.C. Noris², J. Norman¹²⁴, A. Nyman¹⁰⁰, J. Nystrand¹⁸, H. Oeschler⁹³, S. Oh¹³⁶, S.K. Oh⁶⁷, A. Ohlson³⁶, A. Okatan⁶⁹, T. Okubo⁴⁷, L. Olah¹³⁵, J. Oleniacz¹³³, A.C. Oliveira Da Silva¹²⁰, M.H. Oliver¹³⁶, J. Onderwaater⁹⁷, C. Oppedisano¹¹¹, R. Orava⁴⁶, A. Ortiz Velasquez⁶³, A. Oskarsson³⁴, J. Otwinowski¹¹⁷, K. Oyama⁹³, M. Ozdemir⁵³, Y. Pachmayer⁹³, P. Pagano³¹, G. Paić⁶³, C. Pajares¹⁷, S.K. Pal¹³², J. Pan¹³⁴, A.K. Pandey⁴⁸, D. Pant⁴⁸, P. Papcun¹¹⁵, V. Papikyan¹, G.S. Pappalardo¹⁰⁷, P. Pareek⁴⁹, W.J. Park⁹⁷, S. Parmar⁸⁷, A. Passfeld⁵⁴, V. Paticchio¹⁰⁴, R.N. Patra¹³², B. Paul¹⁰¹, T. Peitzmann⁵⁷, H. Pereira Da Costa¹⁵, E. Pereira De Oliveira Filho¹²⁰, D. Peresunko^{100,76}, C.E. Pérez Lara⁸¹, E. Perez Lezama⁵³, V. Peskov⁵³, Y. Pestov⁵, V. Petráček⁴⁰, V. Petrov¹¹², M. Petrovici⁷⁸, C. Petta²⁹, S. Piano¹¹⁰, M. Pikna³⁹, P. Pillot¹¹³, O. Pinazza^{105,36}, L. Pinsky¹²², D.B. Piyarathna¹²², M. Płoskoń⁷⁴, M. Planinic¹²⁹, J. Pluta¹³³, S. Pochybova¹³⁵, P.L.M. Podesta-Lerma¹¹⁹, M.G. Poghosyan^{86,84}, B. Polichtchouk¹¹², N. Poljak¹²⁹, W. Poonsawat¹¹⁴, A. Pop⁷⁸, S. Porteboeuf-Houssais⁷⁰, J. Porter⁷⁴, J. Pospisil⁸³, S.K. Prasad⁴, R. Preghenella^{36,105}, F. Prino¹¹¹, C.A. Pruneau¹³⁴, I. Pshenichnov⁵⁶, M. Puccio¹¹¹, G. Puddu²⁵, P. Pujahari¹³⁴, V. Punin⁹⁹, J. Putschke¹³⁴, H. Qvigstad²², A. Rachevski¹¹⁰, S. Raha⁴, S. Rajput⁹⁰, J. Rak¹²³, A. Rakotozafindrabe¹⁵, L. Ramello³², F. Rami⁵⁵, R. Raniwala⁹¹, S. Raniwala⁹¹, S.S. Räsänen⁴⁶, B.T. Rascanu⁵³, D. Rathee⁸⁷, K.F. Read¹²⁵, J.S. Real⁷¹, K. Redlich⁷⁷, R.J. Reed¹³⁴, A. Rehman¹⁸, P. Reichelt⁵³, F. Reidt^{93,36}, X. Ren⁷, R. Renfordt⁵³, A.R. Reolon⁷², A. Reshetin⁵⁶, F. Rettig⁴³, J.-P. Revol¹², K. Reygers⁹³, V. Riabov⁸⁵, R.A. Ricci⁷³, T. Richert³⁴, M. Richter²², P. Riedler³⁶, W. Riegler³⁶, F. Riggi²⁹, C. Ristea⁶², A. Rivetti¹¹¹, E. Rocco⁵⁷, M. Rodríguez Cahuantzi², A. Rodríguez Manso⁸¹, K. Røed²², E. Rogochaya⁶⁶, D. Rohr⁴³, D. Röhrich¹⁸, R. Romita¹²⁴, F. Ronchetti⁷², L. Ronflette¹¹³, P. Rosnet⁷⁰, A. Rossi^{30,36}, F. Roukoutakis⁸⁸, A. Roy⁴⁹, C. Roy⁵⁵, P. Roy¹⁰¹, A.J. Rubio Montero¹⁰, R. Rui²⁶, R. Russo²⁷, E. Ryabinkin¹⁰⁰, Y. Ryabov⁸⁵, A. Rybicki¹¹⁷, S. Sadovsky¹¹²,

K. Šafařík³⁶, B. Sahlmuller⁵³, P. Sahoo⁴⁹, R. Sahoo⁴⁹, S. Sahoo⁶¹, P.K. Sahu⁶¹, J. Saini¹³², S. Sakai⁷², M.A. Saleh¹³⁴, C.A. Salgado¹⁷, J. Salzwedel²⁰, S. Sambyal⁹⁰, V. Samsonov⁸⁵, X. Sanchez Castro⁵⁵, L. Šándor⁵⁹, A. Sandoval⁶⁴, M. Sano¹²⁸, D. Sarkar¹³², E. Scapparone¹⁰⁵, F. Scarlassara³⁰, R.P. Scharenberg⁹⁵, C. Schiaua⁷⁸, R. Schicker⁹³, C. Schmidt⁹⁷, H.R. Schmidt³⁵, S. Schuchmann⁵³, J. Schukraft³⁶, M. Schulc⁴⁰, T. Schuster¹³⁶, Y. Schutz^{113,36}, K. Schwarz⁹⁷, K. Schweda⁹⁷, G. Scioli²⁸, E. Scomparin¹¹¹, R. Scott¹²⁵, J.E. Seger⁸⁶, Y. Sekiguchi¹²⁷, D. Sekihata⁴⁷, I. Selyuzhenkov⁹⁷, K. Senosi⁶⁵, J. Seo^{96,67}, E. Serradilla^{64,10}, A. Sevcenco⁶², A. Shabanov⁵⁶, A. Shabetai¹¹³, O. Shadura³, R. Shahoyan³⁶, A. Shangaraev¹¹², A. Sharma⁹⁰, M. Sharma⁹⁰, M. Sharma⁹⁰, N. Sharma^{125,61}, K. Shigaki⁴⁷, K. Shtejer^{9,27}, Y. Sibiriyak¹⁰⁰, S. Siddhanta¹⁰⁶, K.M. Sielewicz³⁶, T. Siemiarczuk⁷⁷, D. Silvermyr^{84,34}, C. Silvestre⁷¹, G. Simatovic¹²⁹, G. Simonetti³⁶, R. Singaraju¹³², R. Singh⁷⁹, S. Singha^{132,79}, V. Singhal¹³², B.C. Sinha¹³², T. Sinha¹⁰¹, B. Sitar³⁹, M. Sitta³², T.B. Skaali²², M. Slupecki¹²³, N. Smirnov¹³⁶, R.J.M. Snellings⁵⁷, T.W. Snellman¹²³, C. Sogaard³⁴, R. Soltz⁷⁵, J. Song⁹⁶, M. Song¹³⁷, Z. Song⁷, F. Soramel³⁰, S. Sorensen¹²⁵, M. Spacek⁴⁰, E. Spiriti⁷², I. Sputowska¹¹⁷, M. Spyropoulou-Stassinaki⁸⁸, B.K. Srivastava⁹⁵, J. Stachel⁹³, I. Stan⁶², G. Stefanek⁷⁷, M. Steinpreis²⁰, E. Stenlund³⁴, G. Steyn⁶⁵, J.H. Stiller⁹³, D. Stocco¹¹³, P. Strmen³⁹, A.A.P. Suaide¹²⁰, T. Sugitate⁴⁷, C. Suire⁵¹, M. Suleymanov¹⁶, R. Sultanov⁵⁸, M. Šumbera⁸³, T.J.M. Symons⁷⁴, A. Szabo³⁹, A. Szanto de Toledo^{120,i}, I. Szarka³⁹, A. Szczepankiewicz³⁶, M. Szymanski¹³³, U. Tabassam¹⁶, J. Takahashi¹²¹, G.J. Tambave¹⁸, N. Tanaka¹²⁸, M.A. Tangaro³³, J.D. Tapia Takaki^{iii,51}, A. Tarantola Peloni⁵³, M. Tarhini⁵¹, M. Tariq¹⁹, M.G. Tarzila⁷⁸, A. Tauro³⁶, G. Tejada Muñoz², A. Telesca³⁶, K. Terasaki¹²⁷, C. Terrevoli^{30,25}, B. Teyssier¹³⁰, J. Thäder^{74,97}, D. Thomas¹¹⁸, R. Tieulent¹³⁰, A.R. Timmins¹²², A. Toia⁵³, S. Trogolo¹¹¹, V. Trubnikov³, W.H. Trzaska¹²³, T. Tsuji¹²⁷, A. Tumkin⁹⁹, R. Turrisi¹⁰⁸, T.S. Tveter²², K. Ullaland¹⁸, A. Uras¹³⁰, G.L. Usai²⁵, A. Utrobicic¹²⁹, M. Vajzer⁸³, M. Vala⁵⁹, L. Valencia Palomo⁷⁰, S. Vallero²⁷, J. Van Der Maarel⁵⁷, J.W. Van Hoorne³⁶, M. van Leeuwen⁵⁷, T. Vanat⁸³, P. Vande Vyvre³⁶, D. Varga¹³⁵, A. Vargas², M. Vargyas¹²³, R. Varma⁴⁸, M. Vasileiou⁸⁸, A. Vasiliev¹⁰⁰, A. Vauthier⁷¹, V. Vechernin¹³¹, A.M. Veen⁵⁷, M. Veldhoen⁵⁷, A. Velure¹⁸, M. Venaruzzo⁷³, E. Vercellin²⁷, S. Vergara Limón², R. Vernet⁸, M. Verweij^{134,36}, L. Vickovic¹¹⁶, G. Viesti^{30,i}, J. Viinikainen¹²³, Z. Vilakazi¹²⁶, O. Villalobos Baillie¹⁰², A. Vinogradov¹⁰⁰, L. Vinogradov¹³¹, Y. Vinogradov^{99,i}, T. Virgili³¹, V. Vislavicius³⁴, Y.P. Viyogi¹³², A. Vodopyanov⁶⁶, M.A. Völkl⁹³, K. Voloshin⁵⁸, S.A. Voloshin¹³⁴, G. Volpe^{135,36}, B. von Haller³⁶, I. Vorobyev^{37,92}, D. Vranic^{36,97}, J. Vrláková⁴¹, B. Vulpescu⁷⁰, A. Vyushin⁹⁹, B. Wagner¹⁸, J. Wagner⁹⁷, H. Wang⁵⁷, M. Wang^{7,113}, Y. Wang⁹³, D. Watanabe¹²⁸, Y. Watanabe¹²⁷, M. Weber³⁶, S.G. Weber⁹⁷, J.P. Wessels⁵⁴, U. Westerhoff⁵⁴, J. Wiechula³⁵, J. Wikne²², M. Wilde⁵⁴, G. Wilk⁷⁷, J. Wilkinson⁹³, M.C.S. Williams¹⁰⁵, B. Windelband⁹³, M. Winn⁹³, C.G. Yaldo¹³⁴, H. Yang⁵⁷, P. Yang⁷, S. Yano⁴⁷, Z. Yin⁷, H. Yokoyama¹²⁸, I.-K. Yoo⁹⁶, V. Yurchenko³, I. Yushmanov¹⁰⁰, A. Zaborowska¹³³, V. Zaccaro⁸⁰, A. Zaman¹⁶, C. Zampolli¹⁰⁵, H.J.C. Zanoli¹²⁰, S. Zaporozhets⁶⁶, N. Zardoshti¹⁰², A. Zarochentsev¹³¹, P. Závada⁶⁰, N. Zaviyalov⁹⁹, H. Zbroszczyk¹³³, I.S. Zgura⁶², M. Zhalov⁸⁵, H. Zhang^{18,7}, X. Zhang⁷⁴, Y. Zhang⁷, C. Zhao²², N. Zhigareva⁵⁸, D. Zhou⁷, Y. Zhou^{80,57}, Z. Zhou¹⁸, H. Zhu^{18,7}, J. Zhu^{7,113}, X. Zhu⁷, A. Zichichi^{28,12}, A. Zimmermann⁹³, M.B. Zimmermann^{36,54}, G. Zinovjev³, M. Zyzak⁴³

Affiliation notes

ⁱ Deceased

ⁱⁱ Also at: M.V. Lomonosov Moscow State University, D.V. Skobeltsyn Institute of Nuclear Physics, Moscow, Russia

ⁱⁱⁱ Also at: University of Kansas, Lawrence, Kansas, United States

Collaboration Institutes

¹ A.I. Alikhanyan National Science Laboratory (Yerevan Physics Institute) Foundation, Yerevan, Armenia

² Benemérita Universidad Autónoma de Puebla, Puebla, Mexico

³ Bogolyubov Institute for Theoretical Physics, Kiev, Ukraine

⁴ Bose Institute, Department of Physics and Centre for Astroparticle Physics and Space Science (CAPSS), Kolkata, India

⁵ Budker Institute for Nuclear Physics, Novosibirsk, Russia

⁶ California Polytechnic State University, San Luis Obispo, California, United States

⁷ Central China Normal University, Wuhan, China

⁸ Centre de Calcul de l'IN2P3, Villeurbanne, France

⁹ Centro de Aplicaciones Tecnológicas y Desarrollo Nuclear (CEADEN), Havana, Cuba

¹⁰ Centro de Investigaciones Energéticas Medioambientales y Tecnológicas (CIEMAT), Madrid, Spain

- 11 Centro de Investigación y de Estudios Avanzados (CINVESTAV), Mexico City and Mérida, Mexico
- 12 Centro Fermi - Museo Storico della Fisica e Centro Studi e Ricerche “Enrico Fermi”, Rome, Italy
- 13 Chicago State University, Chicago, Illinois, USA
- 14 China Institute of Atomic Energy, Beijing, China
- 15 Commissariat à l’Energie Atomique, IRFU, Saclay, France
- 16 COMSATS Institute of Information Technology (CIIT), Islamabad, Pakistan
- 17 Departamento de Física de Partículas and IGFAE, Universidad de Santiago de Compostela, Santiago de Compostela, Spain
- 18 Department of Physics and Technology, University of Bergen, Bergen, Norway
- 19 Department of Physics, Aligarh Muslim University, Aligarh, India
- 20 Department of Physics, Ohio State University, Columbus, Ohio, United States
- 21 Department of Physics, Sejong University, Seoul, South Korea
- 22 Department of Physics, University of Oslo, Oslo, Norway
- 23 Dipartimento di Elettrotecnica ed Elettronica del Politecnico, Bari, Italy
- 24 Dipartimento di Fisica dell’Università ‘La Sapienza’ and Sezione INFN Rome, Italy
- 25 Dipartimento di Fisica dell’Università and Sezione INFN, Cagliari, Italy
- 26 Dipartimento di Fisica dell’Università and Sezione INFN, Trieste, Italy
- 27 Dipartimento di Fisica dell’Università and Sezione INFN, Turin, Italy
- 28 Dipartimento di Fisica e Astronomia dell’Università and Sezione INFN, Bologna, Italy
- 29 Dipartimento di Fisica e Astronomia dell’Università and Sezione INFN, Catania, Italy
- 30 Dipartimento di Fisica e Astronomia dell’Università and Sezione INFN, Padova, Italy
- 31 Dipartimento di Fisica ‘E.R. Caianiello’ dell’Università and Gruppo Collegato INFN, Salerno, Italy
- 32 Dipartimento di Scienze e Innovazione Tecnologica dell’Università del Piemonte Orientale and Gruppo Collegato INFN, Alessandria, Italy
- 33 Dipartimento Interateneo di Fisica ‘M. Merlin’ and Sezione INFN, Bari, Italy
- 34 Division of Experimental High Energy Physics, University of Lund, Lund, Sweden
- 35 Eberhard Karls Universität Tübingen, Tübingen, Germany
- 36 European Organization for Nuclear Research (CERN), Geneva, Switzerland
- 37 Excellence Cluster Universe, Technische Universität München, Munich, Germany
- 38 Faculty of Engineering, Bergen University College, Bergen, Norway
- 39 Faculty of Mathematics, Physics and Informatics, Comenius University, Bratislava, Slovakia
- 40 Faculty of Nuclear Sciences and Physical Engineering, Czech Technical University in Prague, Prague, Czech Republic
- 41 Faculty of Science, P.J. Šafárik University, Košice, Slovakia
- 42 Faculty of Technology, Buskerud and Vestfold University College, Vestfold, Norway
- 43 Frankfurt Institute for Advanced Studies, Johann Wolfgang Goethe-Universität Frankfurt, Frankfurt, Germany
- 44 Gangneung-Wonju National University, Gangneung, South Korea
- 45 Gauhati University, Department of Physics, Guwahati, India
- 46 Helsinki Institute of Physics (HIP), Helsinki, Finland
- 47 Hiroshima University, Hiroshima, Japan
- 48 Indian Institute of Technology Bombay (IIT), Mumbai, India
- 49 Indian Institute of Technology Indore, Indore (IITI), India
- 50 Inha University, Incheon, South Korea
- 51 Institut de Physique Nucléaire d’Orsay (IPNO), Université Paris-Sud, CNRS-IN2P3, Orsay, France
- 52 Institut für Informatik, Johann Wolfgang Goethe-Universität Frankfurt, Frankfurt, Germany
- 53 Institut für Kernphysik, Johann Wolfgang Goethe-Universität Frankfurt, Frankfurt, Germany
- 54 Institut für Kernphysik, Westfälische Wilhelms-Universität Münster, Münster, Germany
- 55 Institut Pluridisciplinaire Hubert Curien (IPHC), Université de Strasbourg, CNRS-IN2P3, Strasbourg, France
- 56 Institute for Nuclear Research, Academy of Sciences, Moscow, Russia
- 57 Institute for Subatomic Physics of Utrecht University, Utrecht, Netherlands
- 58 Institute for Theoretical and Experimental Physics, Moscow, Russia
- 59 Institute of Experimental Physics, Slovak Academy of Sciences, Košice, Slovakia
- 60 Institute of Physics, Academy of Sciences of the Czech Republic, Prague, Czech Republic
- 61 Institute of Physics, Bhubaneswar, India

- 62 Institute of Space Science (ISS), Bucharest, Romania
- 63 Instituto de Ciencias Nucleares, Universidad Nacional Autónoma de México, Mexico City, Mexico
- 64 Instituto de Física, Universidad Nacional Autónoma de México, Mexico City, Mexico
- 65 iThemba LABS, National Research Foundation, Somerset West, South Africa
- 66 Joint Institute for Nuclear Research (JINR), Dubna, Russia
- 67 Konkuk University, Seoul, South Korea
- 68 Korea Institute of Science and Technology Information, Daejeon, South Korea
- 69 KTO Karatay University, Konya, Turkey
- 70 Laboratoire de Physique Corpusculaire (LPC), Clermont Université, Université Blaise Pascal, CNRS-IN2P3, Clermont-Ferrand, France
- 71 Laboratoire de Physique Subatomique et de Cosmologie, Université Grenoble-Alpes, CNRS-IN2P3, Grenoble, France
- 72 Laboratori Nazionali di Frascati, INFN, Frascati, Italy
- 73 Laboratori Nazionali di Legnaro, INFN, Legnaro, Italy
- 74 Lawrence Berkeley National Laboratory, Berkeley, California, United States
- 75 Lawrence Livermore National Laboratory, Livermore, California, United States
- 76 Moscow Engineering Physics Institute, Moscow, Russia
- 77 National Centre for Nuclear Studies, Warsaw, Poland
- 78 National Institute for Physics and Nuclear Engineering, Bucharest, Romania
- 79 National Institute of Science Education and Research, Bhubaneswar, India
- 80 Niels Bohr Institute, University of Copenhagen, Copenhagen, Denmark
- 81 Nikhef, Nationaal instituut voor subatomaire fysica, Amsterdam, Netherlands
- 82 Nuclear Physics Group, STFC Daresbury Laboratory, Daresbury, United Kingdom
- 83 Nuclear Physics Institute, Academy of Sciences of the Czech Republic, Řež u Prahy, Czech Republic
- 84 Oak Ridge National Laboratory, Oak Ridge, Tennessee, United States
- 85 Petersburg Nuclear Physics Institute, Gatchina, Russia
- 86 Physics Department, Creighton University, Omaha, Nebraska, United States
- 87 Physics Department, Panjab University, Chandigarh, India
- 88 Physics Department, University of Athens, Athens, Greece
- 89 Physics Department, University of Cape Town, Cape Town, South Africa
- 90 Physics Department, University of Jammu, Jammu, India
- 91 Physics Department, University of Rajasthan, Jaipur, India
- 92 Physik Department, Technische Universität München, Munich, Germany
- 93 Physikalisches Institut, Ruprecht-Karls-Universität Heidelberg, Heidelberg, Germany
- 94 Politecnico di Torino, Turin, Italy
- 95 Purdue University, West Lafayette, Indiana, United States
- 96 Pusan National University, Pusan, South Korea
- 97 Research Division and ExtreMe Matter Institute EMMI, GSI Helmholtzzentrum für Schwerionenforschung, Darmstadt, Germany
- 98 Rudjer Bošković Institute, Zagreb, Croatia
- 99 Russian Federal Nuclear Center (VNIIEF), Sarov, Russia
- 100 Russian Research Centre Kurchatov Institute, Moscow, Russia
- 101 Saha Institute of Nuclear Physics, Kolkata, India
- 102 School of Physics and Astronomy, University of Birmingham, Birmingham, United Kingdom
- 103 Sección Física, Departamento de Ciencias, Pontificia Universidad Católica del Perú, Lima, Peru
- 104 Sezione INFN, Bari, Italy
- 105 Sezione INFN, Bologna, Italy
- 106 Sezione INFN, Cagliari, Italy
- 107 Sezione INFN, Catania, Italy
- 108 Sezione INFN, Padova, Italy
- 109 Sezione INFN, Rome, Italy
- 110 Sezione INFN, Trieste, Italy
- 111 Sezione INFN, Turin, Italy
- 112 SSC IHEP of NRC Kurchatov institute, Protvino, Russia
- 113 SUBATECH, Ecole des Mines de Nantes, Université de Nantes, CNRS-IN2P3, Nantes, France
- 114 Suranaree University of Technology, Nakhon Ratchasima, Thailand

- 115 Technical University of Košice, Košice, Slovakia
- 116 Technical University of Split FESB, Split, Croatia
- 117 The Henryk Niewodniczanski Institute of Nuclear Physics, Polish Academy of Sciences, Cracow, Poland
- 118 The University of Texas at Austin, Physics Department, Austin, Texas, USA
- 119 Universidad Autónoma de Sinaloa, Culiacán, Mexico
- 120 Universidade de São Paulo (USP), São Paulo, Brazil
- 121 Universidade Estadual de Campinas (UNICAMP), Campinas, Brazil
- 122 University of Houston, Houston, Texas, United States
- 123 University of Jyväskylä, Jyväskylä, Finland
- 124 University of Liverpool, Liverpool, United Kingdom
- 125 University of Tennessee, Knoxville, Tennessee, United States
- 126 University of the Witwatersrand, Johannesburg, South Africa
- 127 University of Tokyo, Tokyo, Japan
- 128 University of Tsukuba, Tsukuba, Japan
- 129 University of Zagreb, Zagreb, Croatia
- 130 Université de Lyon, Université Lyon 1, CNRS/IN2P3, IPN-Lyon, Villeurbanne, France
- 131 V. Fock Institute for Physics, St. Petersburg State University, St. Petersburg, Russia
- 132 Variable Energy Cyclotron Centre, Kolkata, India
- 133 Warsaw University of Technology, Warsaw, Poland
- 134 Wayne State University, Detroit, Michigan, United States
- 135 Wigner Research Centre for Physics, Hungarian Academy of Sciences, Budapest, Hungary
- 136 Yale University, New Haven, Connecticut, United States
- 137 Yonsei University, Seoul, South Korea
- 138 Zentrum für Technologietransfer und Telekommunikation (ZTT), Fachhochschule Worms, Worms, Germany